NTNU – Trondheim
Norwegian University of
Science and Technology

Duktilitetsgrenser for rørkutepunkt

Yao Ma

Marine Technology
Submission date: June 2013
Supervisor: Jørgen Amdahl, IMT

Norwegian University of Science and Technology
Department of Marine Technology

Abstract

The nonlinear computer program USFOS is used extensively by oil and engineering companies worldwide to evaluate the ultimate limit strength and accidental limit state behaviour of offshore structures, notably in conjunction with reassessment of existing platforms. In this context it is often necessary to take into account strength reserves on both components and connections (joints). Generally the nonlinear behaviour of components in the form of buckling or large deflection, plastic bending is well known, while the behaviour of tubular joints during extreme plastic deformations is more uncertain. To large degree one has to rely on relatively few experimental data. MSL in UK has developed joint strength formulas expressed as nonlinear P-d curves. Such curves have been implemented in USFOS, but they give sometimes strange results, e.g.- the ductility limit is reached before ultimate strength. Ductility limits are also only given for axial forces and not bending moments. An alternative to physical testing is to perform virtual experiments by means of nonlinear finite element analysis. Provided that simulations are verified against available experimental data, parametric studies of various geometrical configurations and load conditions may expand the data basis. The objective of the work is to perform nonlinear analysis with ABAQUS of various joints and contribute to the development of the data basis. The thesis is a continuation of the specialization project done in 9th semester.

Simulation of joints with ABAQUS is performed to verify the procedure with respect to force-deformation behaviour and strain development. Single joints and the same joints as a part of a frame system plane frame system have been simulated. In this paper, non-linear analysis with ABAQUS of X-joints is performed and the simulation results are verified against existed data and studies. Conclusions and further recommendations are given.

The results show that behavior of the joint is different when analyzed independently from when in frame system. The reason is that when a single joint is analyzed, the force doesn’t change direction. While in a frame system, the braces has a significant influence to the joint, as the braces can buckle, rotate, etc. which changes the direction of the force acting on the joints. When the through member is in tension, the other two braces will compress it to a very large extent, which leads to a large strain development. That can also explain why the frame system is more stable when the joint is rotated by 90 degree. It is the most critical condition when the separate braces are in compression, which should be avoided in reality.

Key words: Ductility limits Tubular joints Non-linear Analysis

MASTER THESIS 2013
for
Stud. techn. Ma Yao

Ductility limits of tubular joints
Duktilitetsgrenser for rørkutepunkt

The nonlinear computer program USFOS is used extensively by oil and engineering companies world wide to evaluate the ultimate limit strength and accidental limit state behaviour of offshore structures, notably in conjunction with reassessment of existing platforms. In this context it is often necessary to take into account strength reserves on both components and connections (joints). Generally the nonlinear behaviour of components in the form of buckling or large deflection, plastic bending is well known, while the behaviour of tubular joints during extreme plastic deformations is more uncertain. To large degree one has to rely on relatively few experimental data. MSL in UK has developed joint strength formulas expressed as nonlinear P-d curves. Such curves have been implemented in USFOS, but they give sometimes strange results, e.g.- the ductility limit is reached before ultimate strength. Ductility limits are also only given for axial forces and not bending moments.

An alternative to physical testing is to perform virtual experiments by means of nonlinear finite element analysis. Provided that simulations are verified against available experimental data, parametric studies of various geometrical configurations and load conditions may expand the data basis. The objective of the work is to perform nonlinear analysis with ABAQUS of various joints and contribute to the development of the data basis.

The work is proposed to be carried out in the following steps.

1. Literature study. Describe the characteristic behaviour of tubular joints up to ultimate strength and in the post-ultimate strength region. Establish an overview of experiments that have been conducted and identify needs for additional data. Review of MSL joint strength formulations and how these have been implemented in USFOS
2. Perform simulation of selected experiments with ABAQUS to verify the simulation procedure with respect to force-deformation behaviour and strain development. A mesh size convergence study may be performed.
3. Perform analysis with USFOS and of single joints and the same joints as a part of a frame system plane frame system. Identify the force-deformation relationships for the joints up to initiation of fracture. The USFOS model shall be based on a beam element modelling and nonlinear spring

representation of the joint.

4. Perform analysis of the single and integrated joints studied in pt. 3 using ABAQUS and USFOS using shell finite element modelling of the joints. The critical strain for crack initiation of the joint shall be discussed. The results of pt.3 and pt.4 shall be compared.
5. Compare the results form the numerical simulations with code formulation. Propose modified joint formulations if need be.
6. Conclusions and recommendations for further work

Useful references: OMAE 2008-57650, OMAE2011-49874

Literature studies of specific topics relevant to the thesis work may be included.

The work scope may prove to be larger than initially anticipated. Subject to approval from the supervisors, topics may be deleted from the list above or reduced in extent.

In the thesis the candidate shall present his personal contribution to the resolution of problems within the scope of the thesis work.

Theories and conclusions should be based on mathematical derivations and/or logic reasoning identifying the various steps in the deduction.

The candidate should utilise the existing possibilities for obtaining relevant literature.

Thesis format

The thesis should be organised in a rational manner to give a clear exposition of results, assessments, and conclusions. The text should be brief and to the point, with a clear language. Telegraphic language should be avoided.

The thesis shall contain the following elements: A text defining the scope, preface, list of contents, summary, main body of thesis, conclusions with recommendations for further work, list of symbols and acronyms, references and (optional) appendices. All figures, tables and equations shall be numerated.

The supervisors may require that the candidate, in an early stage of the work, present a written plan for the completion of the work. The plan should include a budget for the use of computer and laboratory resources, which will be charged to the department. Overruns shall be reported to the supervisors.

The original contribution of the candidate and material taken from other sources shall be clearly defined. Work from other sources shall be properly referenced using an acknowledged referencing system.

The report shall be submitted in two copies:

- Signed by the candidate
- The text defining the scope included
- In bound volume(s)
- Drawings and/or computer prints that cannot be bound should be organised in a separate folder.

Ownership

NTNU has according to the present rules the ownership of the thesis. Any use of the thesis has to be approved by NTNU (or external partner when this applies). The department has the right to use the thesis as if a NTNU employee carried out the work, if nothing else has been agreed in advance.

Thesis supervisor

Prof. Jørgen Amdahl

Contact person at DNV:

Atlke Johansen

Deadline: June 10, 2013

Trondheim, January 14, 2013

Jørgen Amdahl

Preface

This report has been developed in my 10th semester at the Department of Marin Technology of Norwegian University of Science and Technology.

The purpose of the report is to perform a simulation of a selected experiment with ABAQUS to verify the simulation procedure with respect to force-deformation behavior and strain development of joint in isolation and joint in frame system.

Finally I would like to thank Prof. Jørgen Amdahl for his supervision and help of this project thesis. I also want to thank Dr. Li Cheng for his help with model building and the use of ABAQUS.

Trondheim, June 3rd , 2013
Ma Yao

Content

Figures

Tables

Nomenclatures

N_{Rd}	The joint design axial resistance
N_{Rd}	The joint design bending moment resistance
f_y	The yield strength of the chord member at the joint
Q_u	Strength factor
Q_f	Chord action factor
$\sigma_{a,Sd}$	Design axial stress in chord
$\sigma_{my,Sd}$	Design in-plane bending stress in chord
$\sigma_{mz,Sd}$	Design out-of-plane bending stress in chord
T_n	Nominal chord member thickness
T_c	Chords can thickness
L_c	Effective total length
k_0	Initial Joint Stiffness

1. Introduction

Over the last decade, there has been substantial revision of the static strength design and assessment provisions for offshore tubular joints. Accurate predictions of the static collapse and push-over analyses of jacket structures become progressively more important due to the increasing number of aging platforms worldwide. In recent years, re-using of platforms originally designed for different environment conditions is gaining acceptance, and this accentuates the need for accurate re-assessment of structural performance. The accuracy of frame analysis depends primarily on three factors: the accurate representation of member behavior, proper modeling of joint behavior and the joint-frame interaction. Simulation of nonlinear member behavior has been developed accurately throughout the years. Realistic representation of the nonlinear joint behavior for many of the joint types used in offshore structures requires further understanding.

Nonlinear computer programs are used extensively by oil and engineering companies worldwide to evaluate the ultimate limit strength and accidental limit state behaviour of offshore structures, notably in conjunction with reassessment of existing platforms. It is often necessary to take into account strength reserves on both components and connections (joints). Generally the nonlinear behaviour of components in the form of buckling or large deflection, plastic bending is well known, while the behaviour of tubular joints during extreme plastic deformations is more uncertain. To large degree one has to rely on relatively few experimental data. MSL in UK has developed joint strength formulas expressed as nonlinear P-d curves. Such curves have been implemented in USFOS, but they give sometimes strange results, e.g. the ductility limit is reached before ultimate strength. Ductility limits are also only given for axial forces and not bending moments.

In this paper, non-linear analysis with ABAQUS of X-joints is performed and the simulation results are verified against existed data and studies. Conclusions and further recommendations are given.

2. Codes, and guidelines

2.1 NORSOK standard N-004 for tubular joints [1]

In this paper, X-joints are mainly considered about, so the properties of X-joints are to be focused.

2.1.1 Definition of geometrical parameters for X-joints

The validity range for application of the equations defined in 2.1 is as follows:
$0.2 \le \beta \le 1.0$
$10 \le \gamma \le 50$
$30° \le \theta \le 90°$
The above geometry parameters are defined in Figure 2.1:

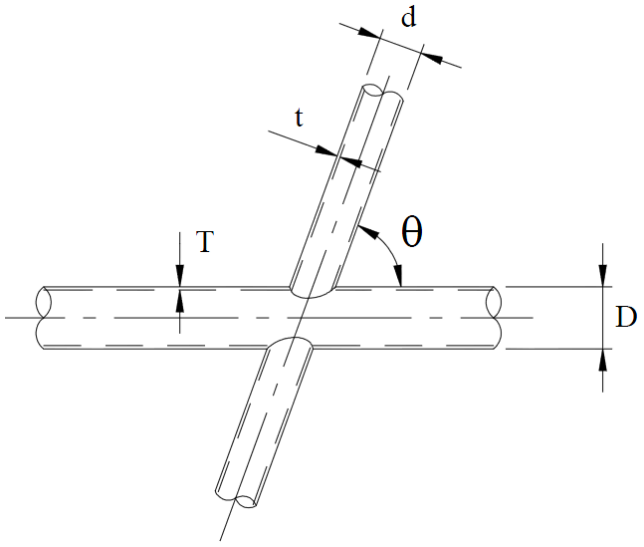

$$\beta = \frac{d}{D}$$

$$\gamma = \frac{D}{2T}$$

$$\tau = \frac{t}{T}$$

$$\alpha = \frac{2L}{D}$$

Figure 2.1 Definition of geometrical parameters for X-joints

2.1.2 Basic resistance

Tubular joints without overlap of principal braces and having no gussets, diaphragms, grout, or stiffeners should be designed using the following guidelines.

The characteristic resistances for simple tubular joints are defined as follows:

$$N_{Rd} = \frac{f_y T^2}{\gamma_M \sin\theta} Q_u Q_f \qquad (2\text{-}1)$$

$$M_{Rd}=\frac{f_y T^2 d}{\gamma_M \sin\theta} Q_u Q_f \qquad (2\text{-}2)$$

where
N_{Rd} = the joint design axial resistance
M_{Rd} = the joint design bending moment resistance
f_y = the yield strength of the chord member at the joint
γ_M = 1.15

2.1.3 Strength factor Q_u

Q_u varies with the joint and action type. As to the X-joints,
Axial tension:
23β for $\beta \le 0.9$
$21+(\beta-0.9)(17\gamma-220)$ for $\beta>0.9$
Axial compression
$(2.8+14\beta)Q_\beta$
Where Q_β is a geometric factor defined by:

$$Q_\beta=\frac{0.3}{\beta(1-0.833\beta)} \quad \text{for } \beta>0.6$$

$$Q_\beta=1.0 \quad \text{for } \beta\le 0.9$$

2.1.4 Chord action factor Q_f

Q_f is a design factor to account for the presence of factored actions in the chord.

$$Q_f=1.0-\lambda A^2$$

where
λ = 0.030 for brace axial force
= 0.045 for brace in-plane bending moment
= 0.021 for brace out-of-plane bending moment
The parameter A is defined as follows:

$$A=C_1\left(\frac{\sigma_{a,Sd}}{f_y}\right)^2+C_2\left(\frac{\sigma_{my,Sd}^2+\sigma_{mz,Sd}^2}{1.62 f_y^2}\right) \qquad (2\text{-}3)$$

Where
$\sigma_{a,Sd}$ = design axial stress in chord
$\sigma_{my,Sd}$ = design in-plane bending stress in chord
$\sigma_{mz,Sd}$ = design out-of-plane bending stress in chord
f_y = yield strength

C_1, C_2 = coefficients depending on joint and load type
For X-joints under brace axial loading C_1=20, C_2=22.
For X-joints under brace moment loading C_1=25, C_2=30.
The chord thickness at the joint should be used in the above calculations. The highest value of A for the chord on either side of the brace intersection should be used.

2.1.5 Design axial resistance for X and Y joints with joint cans

For Y and X joints with axial force and where a joint can is specified, the joint design resistance should be calculated as follows:

$$N_{Rd}=\left(r+(1-r)\left(\frac{T_n}{T_c}\right)^2\right)N_{can,Rd} \qquad (2\text{-}3)$$

Where

$N_{can,Rd}$ N_{Rd} from based on chord can geometric and material properties, including Qf calculated with respect to chord can

T_n Nominal chord member thickness

T_c Chord can thickness

r $L_c/2.5D$ for joints with $\beta \leq 0.9$

$(4\beta - 3)\ L_c/1.5D$ for joints with $\beta > 0.9$

L_c Effective total length

Figure 2.2 shows examples of calculation of L_c. In no case shall r be taken as greater than unity.

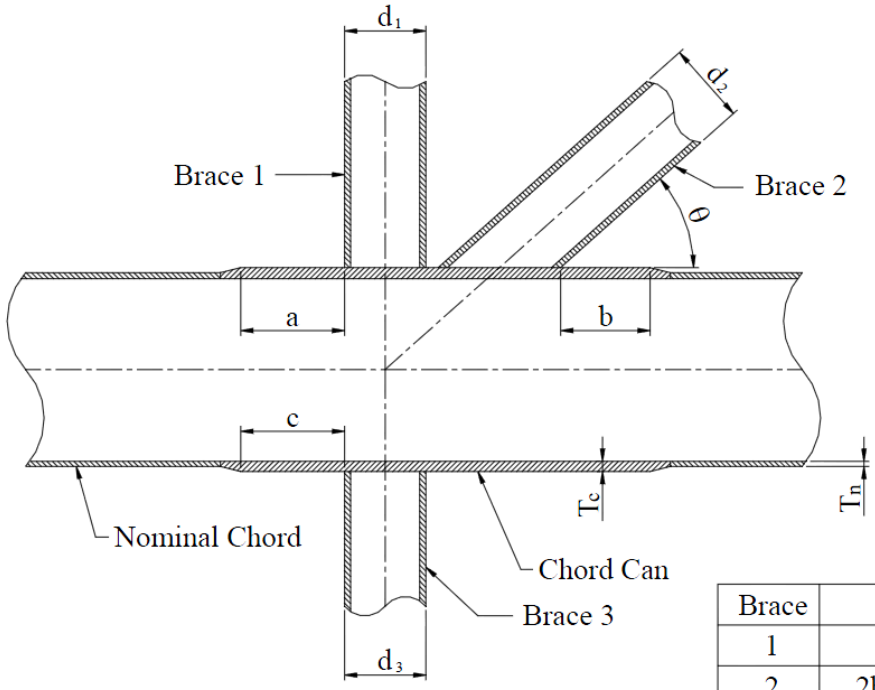

Brace	Length L_c
1	$2a + d_1$
2	$2b + d_2/\sin\theta$
3	$2c + d_3$

Figure 2.2 examples of calculation of L_c

2.2 NORSOK standard N-004 for ductility

It is a fundamental requirement that all failure modes are sufficiently ductile such that the structural behavior will be in accordance with the anticipated model used for determination of the responses. In general all design procedures, regardless of analysis method, will not capture the true structural behavior. Ductile failure modes will allow the structure to redistribute forces in accordance with the presupposed static model. Brittle failure modes shall therefore be avoided or shall be verified to have excess resistance compared to ductile modes, and in this way protect the structure from brittle failure.
The following sources for brittle structural behavior may need to be considered for a steel structure:
1) Unstable fracture caused by a combination of the following factors:
- Brittle material;
- A design resulting in high local stresses;
- The possibilities for weld defects.
2) Structural details where ultimate resistance is reached with plastic deformations only in limited areas, making the global behavior brittle, e.g. partial butt weld loaded transverse to the weld with failure in the weld.
3) Shell buckling.
4) Buckling where interaction between local and global buckling modes occur.
NORSOK standard N-004 Rev. 2, October 2004
NORSOK standard Page 18 of 287
In general a steel structure will be of adequate ductility if the following is satisfied:
1) Material toughness requirements are met, and the design avoids a combination of high local stresses with possibilities of undetected weld defects.
2) Details are designed to develop a certain plastic deflection e.g. partial butt welds subjected to stresses transverse to the weld is designed with excess resistance compared with adjoining plates.
3) Member geometry is selected such that the resistance does not show a sudden drop in capacity when the member is subjected to deformation beyond maximum resistance. An unstiffened shell in cross-section class 4 is an example of a member that may show such an unfavorable resistance deformation relationship. For definition of cross-section class see NS 3472 or NSENV 1993 1-1.
4) Local and global buckling interaction effects are avoided.

2.3 Nonlinear finite element analysis

Non-linear analysis methods have been available for more than 40 years, but it is first during the last decade that these methods have found broad application for offshore structures. This is particularly true when it comes to assessment of existing structures.

Modern codes for offshore structures allow the use of nonlinear methods and are also giving some guidance on how to execute the analyses [2]. Nevertheless, performing non-linear analysis involves many new and demanding challenges both for the analyst and also for those that are reviewing the work.

3. Characteristic behavior of tubular joints and theoretical basis of the thesis

3.1 Brief introduction[3]

The characteristics of load-deformation of X-joints are different under different loading conditions, which represents the input for nonlinear spring models in the frame analysis. Before the ultimate joint strength is reached a bilinear model is employed in consistence with the plastic limit load approach for all loading conditions. For brace axial compression, a re-development of the joint strength occurs at a large deformation level due to the direct contact of the compression braces which are observed in the BOMEL 2D and 3D frame tests. The re-gained strength level equals the brace yield strength, corresponding to $\delta_y = 0.5d_0$.

The strength re-development's initialization depends on the β ratio, as shown in figure 3.1, which defines δ_i at the initial contact of the two braces. For joints with large β ratios, however δ_i becomes impractically small ($\delta_i = 0$ for $\beta = 1.0$). Since the large β joint can undergo certain deformation before the two braces contact one another, δ_i takes the maximum of $0.1d_0$ and $0.5d_0\sin(\cos^{-1}\psi)$. The $0.1d_0$ is a suggested value in the USFOS joint recommendations (USFOS, 2003).

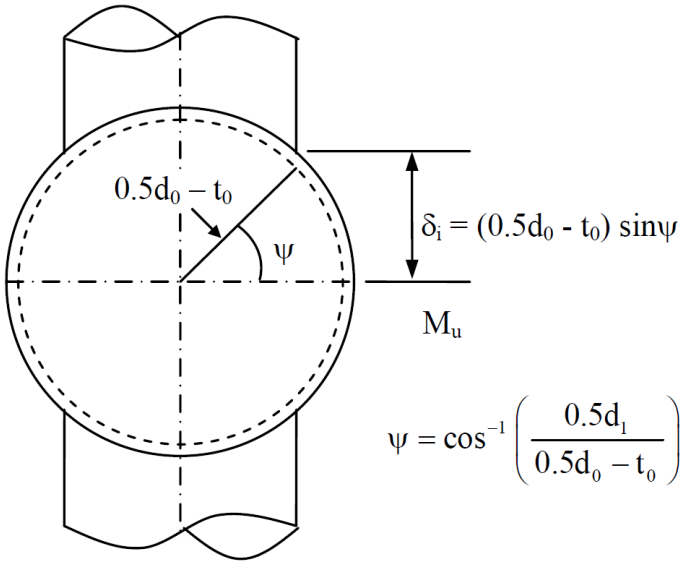

Figure 3.1 Deformation level at the initial contact of two braces for X-joints under brace axial compression.

This is confirmed by an isolated joint analysis by ABAQUS. Contact algorithm is implemented in the analysis so that no self-penetration of the chord inner surface is allowed. The deformation mode at the end of the analysis is shown in Figure 3.2 together with the load deformation response. Once the two braces are in contact, the joint strength will go fast towards the yield strength.

For brace axial tension, the reduction in strength beyond the ultimate load level accounts for the fracture failure in the joint at a large deformation level. As USFOS recommends, the crack initiation is assumed to be at a deformation level of $0.1d_0$. The joint strength beyond the first crack depends on the extent of crack in the joint. An estimation of the cracked joint strength is based on the 30% of the intact cross-section area, or, $P_{cr} = 0.3Pu$, which is arbitrary to simulate the crack failure. It is required by numerical analyses in USFOS that a reduction is needed in the load deformation curve. These load-deformation parameters are investigated in the sensitivity study.

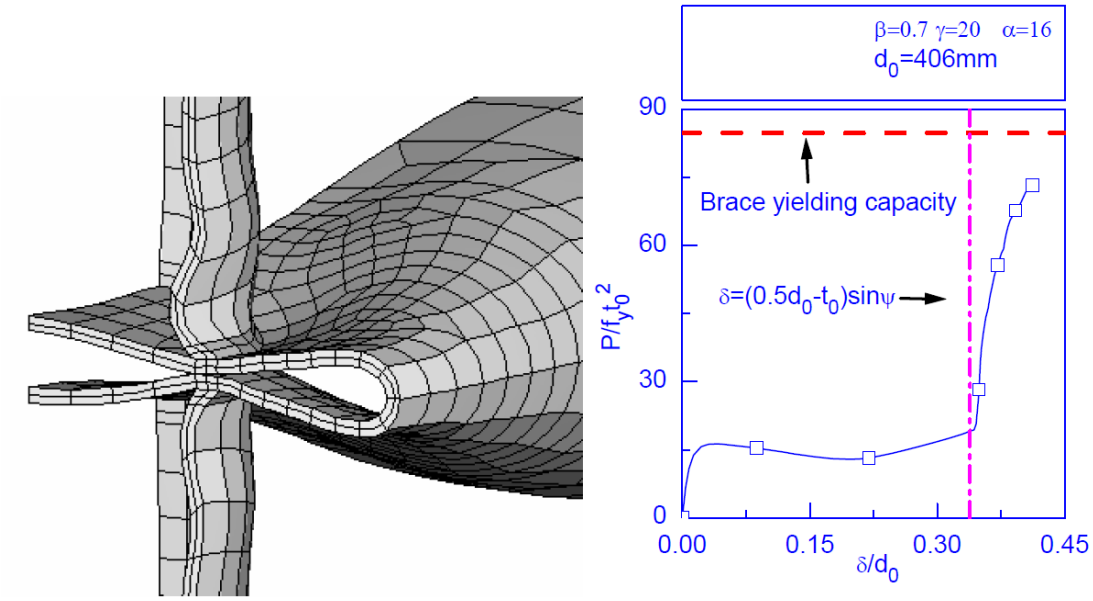

Figure 3.2 X-joint: (a) deformation mode; and (b) load-deformation curve[4].

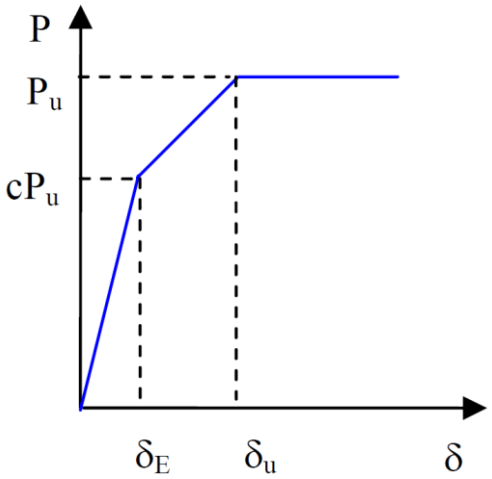

Figure 3.3 Bilinear load-deformation characteristics for nonlinear spring elements [5]

The load-deformation relation re-plotted in Figure 3.3 can be evaluated with reference to the bilinear model. The load level P_E corresponding to the limit of elasticity is assumed to be cP_u, where c defines the ratio of the elastic limit load over the plastic limit load and remains less than 1.0. Since the ultimate joint strength in the current study is based on the plastic limit load at which $\frac{W_P}{W_E}=3.0$. The total work ($W_T=W_P+W_E$) equals ($k_0= cP_u/\delta_E$):

$$W_T=\frac{1}{2}\frac{c^2P_u^2}{k_0}+\frac{1}{2}(1+c)P_u(\delta_u-\delta_E)=\frac{1}{2}\frac{P_u{}^2}{k_0}\left[c^2+(1+c)c(\frac{\delta_u}{\delta_E}-1)\right] \quad (3\text{-}1)$$

$$W_E=\frac{1}{2}\frac{P_u^2}{k_0} \quad (3\text{-}2)$$

$$\frac{W_T}{W_E}=c^2+(c+c^2)\left(\frac{\delta_u}{\delta_E}-1\right)=4 \quad (3\text{-}3)$$

$$\delta_u=\frac{c+4}{c+1}\frac{P_u}{k_0} \quad (3\text{-}4)$$

or

$$c=\frac{4P_u-k_0\delta_u}{k_0\delta_u-P_u} \quad (3\text{-}5)$$

Based on Equation 3-1 to 3-5, $\delta_u$should satisfy the conditions as denoted in equation below, since $0 < c < 1$.

$$\frac{P_u}{0.4k_0}<\delta_u<\frac{P_u}{0.25k_0}$$

The secant stiffness of the joint at ultimate strength level is thus between $0.25k_0$ and $0.4k_0$.

3.2 Initial Joint Stiffness k_0

From the initial steps of the FE analysis we obtain the initial joint stiffness, where the stress-state in the joints remains essentially elastic. The initial joint stiffness is cast in a non-dimensional format based on the non-dimensional strength and deformation parameters adopted in the current study, and the joint stiffness follows a power function of γ. The functions are shown in Equation 3-6 and 3-7[6].

$$k_0=\frac{P\sin\theta/f_yt_0^2}{\delta/t_0}=\frac{P}{\delta}\frac{d_0\sin\theta}{f_yt_0^2} \quad (3\text{-}6)$$

$$k_0(\gamma,\beta)=f_1(\beta)\gamma^{f_2(\beta)} \quad (3\text{-}7)$$

Table 3.1 X-joint stiffness for different brace loads[7]

Loading	$k_0\left(\frac{P}{\delta}\frac{d_0\sin\theta}{f_yt_0^2}\right)$ or $\left(\frac{M}{\phi}\frac{\sin\theta}{f_yt_0^2d}\right)$	FE/k_0		
		Mean	Standard	No. of

			Deviation	data
Axial	$1185\gamma^{(0.8\beta^2+0.15\beta-0.4)}$	1.00	0.08	40
IPB	$(410\beta^2-337\beta+91)\gamma^{(-0.46+1.15)}$	1.00	0.04	15
OPB	$123\beta^{(1.8+0.095\gamma)}\gamma^{(2.9\beta^2-4.4\beta+2.5)}$	1.02	0.05	15

The coefficients in Equation 3-6 and 3-7 are assumed to depend on β, and determined by regression analysis. In Eq. 3-7, $f_1(\beta)$ and $f_2(\beta)$ follow the polynomial relationship. The stiffness formulation k_0 is tabulated in Table 3.1. The statistical comparison with respect to FE data is incorporated in the same table.

3.2 Ultimate Joint Strength

The ultimate strength equation is simplified based on the exact ring model solution proposed by van der Vegte (1995)[8]. The X-joint strength formulation is shown in Equation 3-8 for brace axial compression, axial tension, IPB and OPB respectively. Modifications have been included to incorporate the dependence for thick-walled joints.

$$\frac{P_u \sin\theta}{f_y t_0^2} = \frac{p_1}{(1-p_2\beta^{\gamma})}\gamma^{(p_3+p_4\beta)} \tag{3-8}$$

$$\frac{M_{u,ipb} \sin\theta}{f_y t_0^2 d_1} = p_1 \beta^{p_2} \gamma^{p_3} \tag{3-9}$$

$$\frac{M_{u,opb} \sin\theta}{f_y t_0^2 d_1} = p_1 \gamma^{f(\beta)} \tag{3-10}$$

Table 3.2 X-joint strength formulation for different brace loads

Loading	$\frac{P_u \sin\theta}{f_y t_0^2}$ or $\frac{M_u \sin\theta}{f_y t_0^2 d_1}$	FE/k_0		
		Mean	Standard Deviation	No. of data
Axial	$\frac{8.8}{(1-0.4\beta^{\gamma})}\gamma^{(-0.2+0.56\beta)}$	0.98	0.08	51
IPB	$3.1\beta\gamma^{0.65}$	1.00	0.07	15
OPB	$3.8\gamma^{0.53\beta^{2.4}}$	0.99	0.08	15

Table 3.2 shows the final equations for X-joints obtained using nonlinear regression analyses. Table 3.2 also shows the statistical comparison of the proposed equation and FE data. The representation for X-joints under tension is based on the ultimate joint

strength instead of the strength corresponding to the first crack, since fracture failure does not become dominant until it achieves a large deformation level, which is different from ISO formulation.

3.3 Coefficients c and δ_u

To form a complete bilinear model, the coefficient c needs to be determined to evaluate P_E (= cP_u) and M_E (= cM_u). For X-joints, a convenient value of 0.8 is assumed for c under all loading conditions.

Table 3.3 Comparison of δ_u by Eq. 8.4 and FE results for X-joints

Loading	No. of data	δ_u or ϕ_u(FE) /δ_u or ϕ_u(Eq. 3-4 & 3-5)	
		Mean	Standard Deviation
Axial	40	0.98	0.08
IPB	15	1.00	0.07
OPB	15	0.99	0.08

The joint deformation δ_u is calculated using Equation 3-4 and compared to the joint deformation obtained from the FE analysis. Table 8.4 shows a good agreement in the deformation level between Equation 3-4 and the FE data, which indicates the appropriateness of the c value assumed.

3.3 MSL Joint behavior and ductility limits [9]

3.3.1 General

The current joint capacity check included in USFOS covers simple tubular joint and is based on capacity formulas and description of the joint behavior developed during the MSL Joint Industry Projects. In addition to the original MSL formulations, code variants from Norsok, ISO and API are also implemented.

3.3.2 MSL variants

The MSL Joint Industry Projects developed several sets of capacity formulas based on a large database of laboratory test results.

The original MSL versions include
•Mean Ultimate
•Characteristic Ultimate
•Characteristic First Crack

Mean Ultimate represents the statistical mean failure of the joints tested (top of the force-displacement curve, "the most probable failure load").
Characteristic Ultimate is based on the same data, but the as the title say, the capacity is reduced in order to account for the spreading in the test results.
Characteristic First Crack is in most cases equal to "Characteristic Ultimate" but is further reduced in some cases in order to avoid degradation of the joint for repeated loading. This version is recommended for structures subjected to repeated load actions, e.g. wave loading.

3.3.3 Code variants

Note that the first crack characteristic capacity equations in the code variants are implemented in USFOS excluding the safety factors given in the codes. The additional safety level required by the code for the various limit states analyzed must in USFOS be included on the load side (by increasing the applied loads).

The MSL capacity check formulas have been adopted and adjusted by Norsok and ISO. The code variants are based on the MSL First Crack capacity formulas. The (Q_u) expressions are nearly identical, but the correction factor for chord utilization differs from MSL. Also the interaction between axial force, in-plane and out-of-plane bending differs. The code variants put more weight on the out-of plane bending component.

The formulas are also based on the MSL database, however, the database used to develop the latest joint capacity equations for API RP2A are extended using results from FE analyses. API RP2A (21st edition) is currently (2009) the most updated code with respect to joint capacity.

In this paper Norsok-004 is discussed and the other codes are neglected.

3.3.4 Joint P-D curves

The following expressions show the original MSL proposed relationship between the joint force/moments and joint displacements/rotations.

$$P=\phi P_u\left(1-A\left[1-\left(1+\frac{1}{\sqrt{A}}\right)\exp\left(-B\frac{\delta}{\phi Q_f F_y D}\right)\right]^2\right) \quad (3\text{-}11)$$

$$M=\phi M_u\left(1-A\left[1-\left(1+\frac{1}{\sqrt{A}}\right)\exp\left(-B\frac{\theta}{\phi Q_f F_y}\right)\right]^2\right) \quad (3\text{-}12)$$

Table 3.4 Coefficients A and B

Joint Type	Load Type	Coefficient	
		A	B
X	Compression	$\left((\gamma-4)\sin^3\theta\right)/62$	$600\beta+13500$
	Tension	0.001	$12000\beta + 1200$
	IPB	0.001	$9700\beta + 6700$
	OPB	0.001	$8600\beta + 1200$

Where γ and β are the parameters shown in section 2.1.1.

3.3.5 MSL Ductility limits

The MSL proposed ductility limits of X-joints for axial deflection are:
Mean:

$$\frac{\delta}{D}=0.13-0.11\beta$$

Characteristic:

$$\frac{\delta}{D}=0.089-0.075\beta$$

In USFOS, the ductility limit is implemented by reducing the axial joint capacity to a small number for deformations larger than the ductility limit. No formulations are identified for mean and characteristic fracture criteria related to other degrees of freedom.

From the limits it is seen that the ductility limits are very conservative. It is no more than 0.13 times the out diameter. While during the analysis by ABAQUS, it is seen that the joints can deform much larger than the limit before they reach the yield stress limit, which will be shown later.

3.4 The BWH instability criterion[10]

3.4.1 Introduction

When exploring the limits of metal sheets it is important to give reasonable prediction of fracture. This is true for metal forming processes and in crash worthiness analyses where failure may reduce the resistance of a structure significantly. In industrial forming processes, the Keeler–Goodwin approach, see Keeler and Backhofen (1964)[11] and Goodwin (1968)[12], has for many years been the dominating method to estimate failure. In this method, the principal strains $(\varepsilon_1,\varepsilon_2)$ at incipient plastic instability are plotted in a forming limit diagram (FLD). Figure 3.4 illustrates an example of such a diagram.

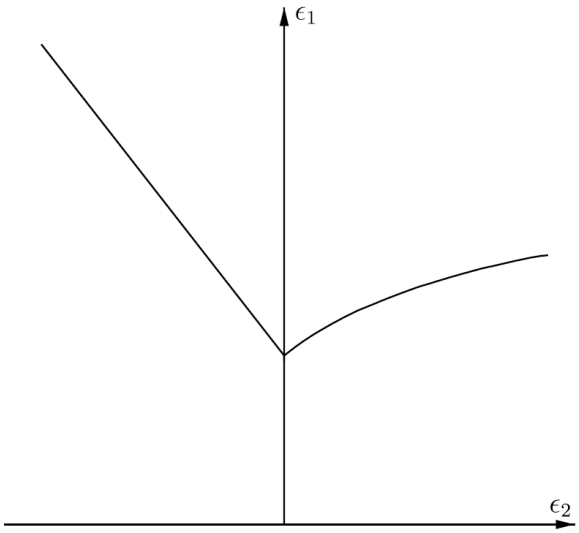

Figure 3.4 Typical forming limit diagram.

Proportional strain paths are assumed when the FLD is established which means that the ratio between the minor principal strain rate $\dot{\varepsilon}_2$ and major principal strain rate $\dot{\varepsilon}_1$ remains constant during deformation. This may not necessarily be the case in processes where large deformation occurs, e.g., industrial metal forming applications and sheet metal deformation in collision processes. The loading path may be changed due to various effects, such as material hardening, changed specimen geometry and contact. Several authors have reported that non-proportional strain paths may change the forming limits of materials, e.g., Ghosh and Laukonis (1976)[13] and Graf and Hosford (1993)[14]. Awareness of this effect was raised during the 1970s, through FLDs derived from experiments on pre-strained specimens, e.g., Ghosh and Laukonis (1976)[15]. Later documentation on this was published during the 1980s and 1990s; see for example Rocha et al. (1985)[16], Graf and Hosford (1993)[17]. Although its generality may be questioned, the Keeler–Goodwin method has not changed much from its initial form. Reasons for this may be that FLDs are intuitive and easy to use. More complex methods require more resources, both from computers and the ones

applying them.

A simple alternative to strain based FLDs is stress based FLDs. Such diagrams were first presented by Arrieux et al. (1982)[18], and later by Stoughton (2000, 2001)[19], Stoughton and Zhu (2004)[20] and Wu et al. (2005)[21]. The idea is that stress based criteria remains more or less unaffected by altered strain paths. Furthermore, the nature of this type of formulation is simple and easily implemented into a finite element (FE) code.

The BWH criterion is meant to offer a simplified way to estimate the onset of local necking. The verification of the BWH criterion is carried out in two separate series of analyses. The first one is a set of analytical considerations, which is compared with FLDs found in literature. The second set of analyses is performed numerically using the finite element code LS-DYNA, see Hallquist (2007a, b)[22]. The finite element simulations are further compared with benchmark tests (large scale bulge tests) provided by Tornqvist (2003)[23].

3.4.2 The BWH instability criterion

The forming limit diagram, as it is most often presented, is an intuitive way of displaying the limits of materials. However, as it has been highlighted, it is only strictly valid for proportional straining, i.e., the strain rate ratio $\beta=\dot{\varepsilon}_2/\dot{\varepsilon}_1$ remains constant. Ghosh and Laukonis (1976)[24] and Graf and Hosford (1993)[25] have shown that for non-linear strain paths, the FLD may change. One simplified way of circumventing this problem is to adopt stress based forming limit curves (FLC). This methodology has been strongly argumented for by Stoughton, see for example Stoughton (2000, 2001)[26] and Stoughton and Zhu (2004)[27]. Stresses can be directly coupled to the plastic strain rates through the relations between the strain rates and the conditions for yielding and plastic flow. If the yield function and the potential for plastic flow are assumed identical, the relations between strain rates and stresses can be found from the associated flow rule

$$\dot{\varepsilon}_{ij}=\dot{\lambda}\frac{\partial f}{\partial \sigma_{ij}} \tag{3-13}$$

where $\dot{\varepsilon}_{ij}$ and σ_{ij} denotes plastic strain rate and stress tensor on index form, k is the plastic multiplier, and f describes the yield function. If J_2 flow theory and plane stress conditions are assumed, the relation between the strain rate ratio b and the principal stresses σ_1 and σ_2 can be expressed as

$$\alpha=\frac{\sigma_2}{\sigma_1}=\frac{1+2\beta}{\beta+2} \tag{3-14}$$

Note that only for plastic strains is this relation valid. Elastic strains are neglected, which is reasonable since plastic strains are much larger. In Figure 3.5, an example of

a strain based FLD (a) and a stress FLD (b) is shown. The difference between these is that the stress based FLC remains fixed in the stress space for non-linear strain paths, while the strain based FLC may change for various combinations of non-proportional straining.

3.4.2.1 Hill's local necking criterion

Hill (1952)[28] proposed a criterion for local necking in the negative β regime. He assumed that a local neck will form with an angle ϕ to the direction of the major principal stress. Within this neck, the strain increments along the narrow necking band will be zero. The orientation of the neck may be expressed as $\phi=\tan^{-1}\left(1/\sqrt{-\beta}\right)$, which yields rational results only for negative values of b. At the instant a neck is formed, the effects from strain hardening and the diminution in thickness balance each other exactly. This means that the fractions within the material reach a maximum value at the point of local necking. This gives traction increments equal to zero, $dT_1=0$, at the point of necking, which leads to the following local necking criterion

$$\frac{d\sigma_1}{d\varepsilon_1}=\sigma_1(1+\beta) \tag{3-15}$$

Assuming that the material stress–strain curve can be represented by the power law expression, $\sigma_{eq}=K\varepsilon_{eq}^{n}$, where (K, n) are material parameters and (σ_{eq}, ε_{eq}) are the equivalent stress and strain, and that proportionality between stress rates and stresses can be assumed, i.e.,

$$\alpha=\frac{\dot{\sigma}_2}{\dot{\sigma}_1}=\frac{\sigma_2}{\sigma_1} \tag{3-16}$$

the equivalent strain at local necking can be expressed as

$$\varepsilon_{eq}=\frac{2n}{\sqrt{3}}\frac{\sqrt{\beta^2+\beta+1}}{1+\beta} \tag{3-17}$$

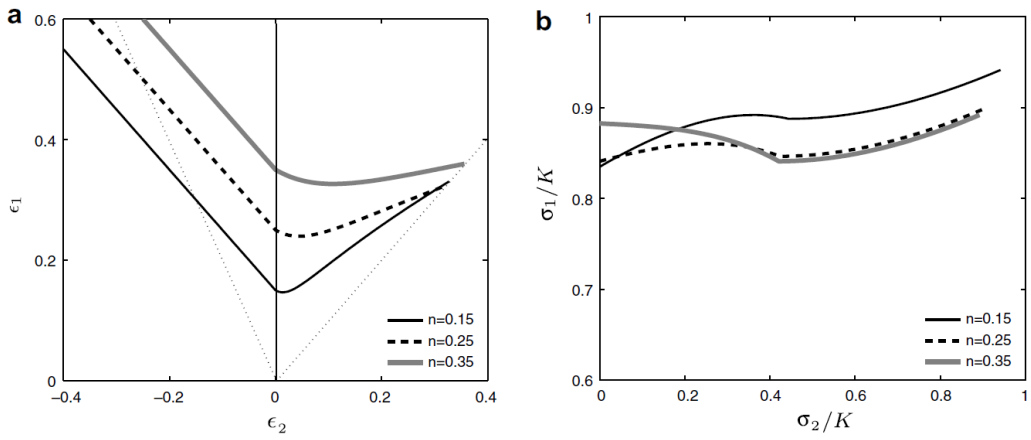

Figure 3.5 Forming limit diagrams in (a) strain space, (b) stress space. Both figures

illustrate the same materials. Note that the figure (b) is normalized by the powerlaw parameter K in $\sigma_{eq}=K\varepsilon_{eq}^{n}$, where ($\sigma_{eq}$, ε_{eq}) are the equivalent stress and strain

If proportional straining is assumed, the familiar strain based Hill's expression appears

$$\varepsilon_1^*=\frac{\hat{\varepsilon}_1}{1+\beta} \tag{3-18}$$

Here $\hat{\varepsilon}_1$ is equal to the power law exponent n, although measured values may sometimes yield better correlation with experiments. As equation Eq. 3-18 is based on proportionality it has limited use. Alternatively, a path independent stress based FLC may be found directly from Eq. 3-17 and the power law expression. This gives the equivalent stress at local necking (note that also here refers to the power law exponent n)

$$\varepsilon_{eq}=\left(\frac{2\hat{\varepsilon}_1}{\sqrt{3}}\frac{\sqrt{\beta^2+\beta+1}}{1+\beta}\right)^{n} \tag{3-19}$$

This results in the following major principal stress

$$\sigma_1=\frac{2K}{\sqrt{3}}\frac{1+\frac{\beta}{2}}{\sqrt{\beta^2+\beta+1}}\left(\frac{2}{\sqrt{3}}\frac{\hat{\varepsilon}_1}{1+\beta}\sqrt{\beta^2+\beta+1}\right)^{n} \tag{3-20}$$

A similar derivation has been shown by Stoughton and Zhu (2004)[29].

3.4.2.2 The Bressan–Williams shear instability criterion

Hill's local necking criterion yields only rational results for negative β values. In the positive regime, other methods of estimating the onset of local necking are needed. A popular solution to this goes through the methodology established by Marciniak and Kuczynski (1967) (M–K)[30]. This procedure introduces pre-existing defects within the material, which trigger local necking. The defects are often introduced as a groove within a material element. During deformation, the strain field is solved incrementally. Local necking is initiated once the material within the groove starts to strain at a significantly higher rate than the surrounding material and the strain rate ratio b within the emerging neck approaches zero (plane strain). The M–K method describes in a physical way the initial stage of local necking and as for stress based approaches, it does handle non-proportional straining. The drawback, however, is that it becomes computationally demanding if used in finite element analyses. Either one has to apply a high number of small elements in order to include small imperfections, or the M–K procedure needs to be introduced into each finite element. Hence, a much simpler stress based instability criterion known as the Bressan–Williams criterion (BW) is adopted, Bressan and Williams (1983)[31]. Contrary to the M–K method, the BW

criterion may be solved analytically and can be used for failure estimation with reasonable precision at a low cost.

In plasticity, the main mechanism of deformation comes from slip arising from shear on certain preferred combinations of crystallographic planes. Furthermore, it has been observed by experiments that failure planes in sheet metal lie close to the direction of maximum shear stress, see Bressan and Williams (1983)[32]. It is therefore reasonable to assume that the instability may take place before any visual signs of local necking. Thus, a shear stress based instability criterion may well be useful in estimating the point of local necking. As presented by Bressan and Williams (1983), the BW criterion has a simple expression and has been applied with good results. The basis for the BW expression follows three basic assumptions. First of all, the shear instability is initiated in the direction through the thickness at which the material element experiences no change of length. This indicates a critical through thickness shear direction. Secondly, the instability is triggered by a local shear stress which exceeds a critical value. This means that the initiation of local necking is described as a material property. Finally, elastic strains are neglected. This is reasonable since the elastic strains are small compared to the plastic strains at local necking.

From Fig. 3, and from the assumptions above, a mathematical formulation for the BW criterion can be found. As illustrated in Figure 3.6a, the inclined plane through the element thickness at which shear instability occurs (indicated by the plane normal x_n) forms an angle $\pi/2-\theta$ to the shell plane. The material experiences zero elongation in this direction, indicating that $\dot{\varepsilon}_t=0$. This gives the following relation between the angle of the inclined plane and the principal strain rates

$$\dot{\varepsilon}_t=\frac{\dot{\varepsilon}_1+\dot{\varepsilon}_2}{2}+\frac{\dot{\varepsilon}_1-\dot{\varepsilon}_3}{2}\cos 2\left(\theta+\frac{\pi}{2}\right)=0 \qquad (3\text{-}21)$$

Where $\cos 2(\theta+\pi/2)=\cos 2\theta$, which further gives

$$\cos 2\theta=\frac{\dot{\varepsilon}_1+\dot{\varepsilon}_3}{\dot{\varepsilon}_1-\dot{\varepsilon}_3} \qquad (3\text{-}22)$$

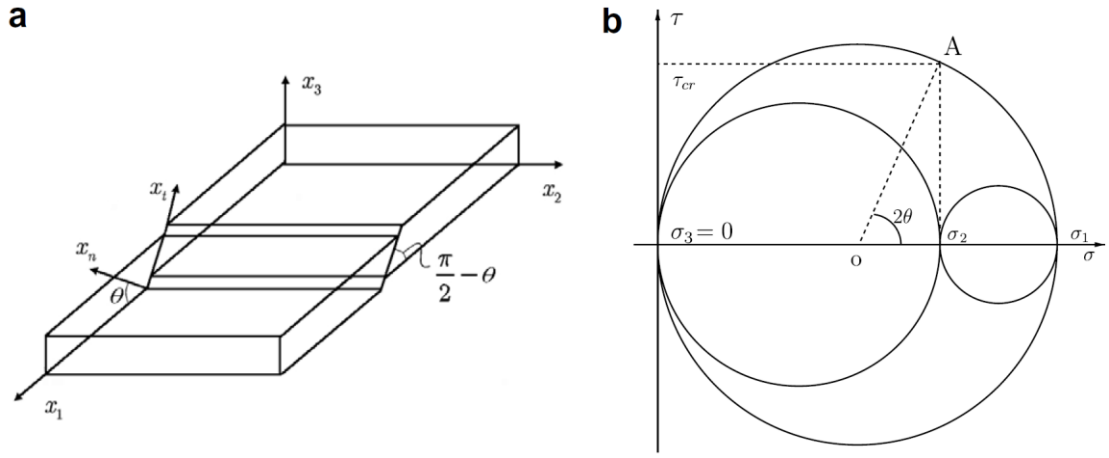

Figure 3.6 (a) Local shear instability in a material element. Note that no elongation

takes place in the xt direction. (b) Shows the stress components in a Mohr's circle.

Assuming plastic incompressibility, $\dot{\varepsilon}_3 = -\dot{\varepsilon}_1(1+\beta)$, the angle θ can be found as a function of the ratio β

$$\cos 2\theta = -\frac{\beta}{2+\beta} \tag{3-23}$$

The corresponding stress state can be obtained from the rules of stress transformation, or simply by drawing up Mohr's circle, Figure 3.6b. This gives the following relation between the inclined plane and the stresses involved

$$\tau_{cr} = \frac{\sigma_1}{2}\sin 2\theta \tag{3-24}$$

where τ_{cr} is the critical shear stress. Finally, equations may be combined into the expression which gives the BW criterion

$$\sigma_1 = \frac{2\tau_{cr}}{\sqrt{1-\left(\frac{\beta}{2+\beta}\right)^2}} \tag{3-25}$$

A similar derivation is given by Brunet and Clerc (2007)[33]. Bressan and Williams initially suggested calibration either from uniaxial tensile tests or biaxial tests. Another alternative may be calibration at plane strain, $\beta = 0$, through notched specimens or simply from Hill's analysis. If the BW criterion is calibrated from Hill's expression at plane strain, the critical BW shear stress takes the following form

$$\tau_{cr} = \frac{1}{\sqrt{3}} K \left(\frac{2}{\sqrt{3}}\hat{\varepsilon}_1\right)^n \tag{3-26}$$

Also here, $\hat{\varepsilon}_1$ is equal to the power law exponent *n*.

3.4.2.3. The Bressan–Williams–Hill criterion

The BW criterion was initially intended for the positive quadrant of the FLD, but the mathematical expression is also valid for negative values. However, as the strain rate ratio becomes negative, the validity of the BW criterion becomes questionable. Hence, in order to cover the full range of β, the Hill and BW criteria have been combined into one criterion, from now on referred to as the BWH criterion. Formulated in terms of the strain rate ratio, β, the criterion reads

$$\sigma_1 = \frac{2K}{\sqrt{3}} \frac{1+\frac{1}{2}\beta}{\sqrt{\beta^2+\beta+1}} \left(\frac{2}{\sqrt{3}} \frac{\hat{\varepsilon}_1}{1+\beta}\sqrt{\beta^2+\beta+1}\right)^n, \qquad \beta \leq 0$$

$$\sigma_1 = \frac{2K}{\sqrt{3}} \frac{\left(\frac{2}{\sqrt{3}}\hat{\varepsilon}_1\right)^n}{\sqrt{1-\left(\frac{\beta}{2+\beta}\right)^2}}, \qquad \text{otherwise}$$

The BWH criterion is illustrated in both strain and stress space in Figure 3.5 for various hardening exponents, *n*.

3.5 Introduction of Nonlinear Analysis[34]

3.5.1. General

Structural analysis, the finite element method included, is based on the following principles:

- Equilibrium (expressed by stresses)
- Kinematic compatibility (expressed by strains)
- Stress-strain relationship

When doing linear analysis it is assumed that displacements are small and the material is linear and elastic. When the displacements are small, the equilibrium equations can be established with reference to the initial configuration, which means that the strains and displacement gradients (derivatives) have linear relation corresponding to Hooke's law.

However when the ultimate strength of structures such that buckle and collapse is to be calculated, small displacements and linear material assumptions are no longer available and accurate. If the change of geometry is accounted for, when establishing the equilibrium equations and calculating the strains from displacements, a geometrical nonlinear behavior is accounted for. Analogously, material nonlinear behavior is associated with nonlinear stress-strain relationship.

Nonlinearity may be also related to the boundary condition, i.e. when a large displacement leads to contact. Boundary non-linearity occurs in most contact problems, in which two surfaces come into or out of contact. The displacements and stresses of the contacting bodies are usually not linearly dependent on the applied loads. This type of non-linearity may occur even if the material behavior is assumed linear and the displacement are infinitesimal, due to the fact that that the size of the contact area is usually not linearly dependent on the applied loads, i.e. doubling the applied loads does not necessarily produce double the displacement. If the effect of friction is incl-

uded in the analysis, then slick-slip behaviour may occur in the contact area which adds a further nonlinear complexity that is normally dependent on the loading history.

There are several areas where nonlinear stress analysis may be necessary:

- Direct use in design for ultimate and accidental collapse limit states. Modern structural design codes refer to truly ultimate failure modes and not only first yield and analogous modes.
- Use in the assessment of existing *structures* whose integrity may be in doubt due to (a) visible damage (crack, etc.) concern over corrosion or general ageing. The above will largely relate to the ultimate limit state because, in many cases, the serviceability limit state will already have been exceeded and yet key question still remain such as: Is the structure safe? Should it be repaired and if so, how will any proposed strengthening work? Can it be kept in service for a little time longer?
- Use to help to establish the causes of a structural failure.
- Use in code development and *research*: (a) to help to establish simple 'code based' methods of analysis and design, (b) to help understand basic structural behavior and (c) to test the validity of proposed 'material models'.

With the new generation of inexpensive yet powerful computers, solution cost is no longer the major obstacle it has been. However, the complexity of nonlinear stress analysis still remains to provide the 'expert' as well as the unwary novice with many headaches.

Nonlinear analyses are applied in all the ways mentioned above. However, a signify-cant increase in the use of nonlinear stress analyses in the assessment of existing structures is envisaged and eventually in the direct design of more routine structures. This will occur as hardware becomes cheaper and faster and software becomes more robust and user-friendly.

It will simply become easier for an engineer to apply direct analysis rather than code based charts. However, problems will arise because the latter often include 'fiddle factors' relating to experience, uncertainty, etc. The advent of more computer-based analysis procedures will lead to the need for a 'surrounding', probably computer based, 'code' to incorporate the 'partial factors' including those factors (often now hidden) relating to the degree of uncertainty of the analysis. The analysis would have to be directly embedded in a statistical reliability framework.

3.5.2 Nonlinear material behavior

A material is called nonlinear if stresses σ and strains ε are related by a strain

dependent matrix rather than a matrix of constants. Thus the computational difficulty is that equilibrium equations must be written using material properties that depend on strains, but strains are not known in advance. Plastic flow is often a cause of material nonlinearity. The present section deals with formulation of elastic-plastic problems by considering the one dimensional case.

Assume that yielding has already occurred, and then a strain increment $d\varepsilon$ takes place. This strain increment can be regarded as composed of an elastic contribution $d\varepsilon^e$ and a plastic contribution $d\varepsilon^p$so that $d\varepsilon=d\varepsilon^e+d\varepsilon^p$. The corresponding stress increment can be written in various ways

$d\sigma=Ed\varepsilon^e=E(d\varepsilon-d\varepsilon^p)$; $d\sigma=E_t d\varepsilon$;and $d\sigma=H' d\varepsilon^p$

Where H' is called the plastic tangent modulus as given by $\partial\sigma/\partial\varepsilon^p$. Substitution of the first and third into the second yields

$$H'=\frac{1}{\frac{1}{E_t}-\frac{1}{E}} \text{ or } E_t=E\left(1-\frac{E}{E+H'}\right) \qquad (3\text{-}27)$$

where E_t is the tangent modulus. When written in this form, the expression for E_t is similar to a more general expression used for multiaxial states of stress. If E is finite and $E_t=0$, then $H'=0$, and the material is called "elastic-perfectly plastic".

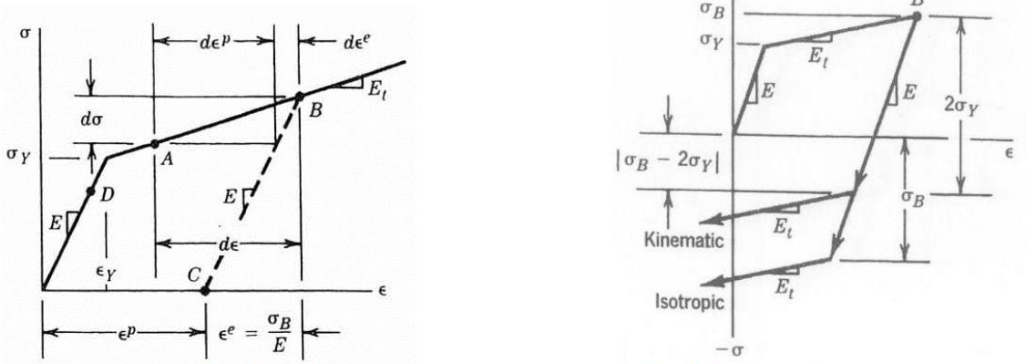

a) Stress-strain plot in uniaxial stress, idealized as two straight lines, where σ_y is the stress at first onset of yielding.

b) Kinematic and isotropic hardening rules.

Figure 3.7 characteristic features of one-dimensional stress-strain relationships.

A summary of elastic-plastic action in uniaxial stress is as follows:

1) The yield criterion states that yielding begins when $|\sigma|$ reaches σ_Y, where in practice σ_Y is usually taken as the tensile yield strength. Subsequent plastic deformations may alter the stress needed to produce renewed or continued yielding; this stress exceeds the initial yield strength σ_Y if $E_t>0$.

2) A hardening rule, which describes how the yield criterion is changes by the history of plastic flow. For example, imagine that the material first has been loaded to point B

and then unloading occurs from point B to point C in Figure 3.7a. With reloading from point C, response will be elastic until $\sigma>\sigma_B$, when renewed yielding occurs. Assume then that unloading occurs from point B and progresses into a reversed loading as shown in Figure 3.7b. If the yielding is assumed to occur at $|\sigma|=\sigma_B$ the hardening is said to be isotropic. However, for common metals, such a rule is in conflict with the observed behavior that yielding reappears at a stress of approximate magnitude $\sigma_B-2\sigma_Y$ when loading is reversed. Accordingly, a better match to observed behavior is provided by the "kinematic hardening" rule, which (for uniaxial stress) says that a total elastic range of $2\sigma_Y$ is preserved.

3) A flow rule can be written in multidimensional problems. It leads to a relation between stress increments $d\sigma$ and strain increments $d\varepsilon$. In uniaxial stress this relation is simply $d\sigma=E_t d\varepsilon$, which describes the increment of stress produced by an increment of strain. Note, however, that if the material has yet to yield or is unloading, then $d\sigma=Ed\varepsilon$, (e.g., Figure 3.7a, complete unloading from point B leads to point C and a permanent strain ε^p).

3.5.3 Solution techniques

While in linear analysis the solution always is unique, this may no longer be the case in non-linear problems. Thus the solution achieved may not necessarily be the solution sought.
The resultant of internal forces can be expressed as

$$\mathbf{R}_{int}=\sum_i \left(\mathbf{a}^i\right)^T \mathbf{S}^i \qquad (3\text{-}28)$$

and the total equilibrium can be expressed as

$$\mathbf{R}_{int}=\mathbf{R} \qquad (3\text{-}29)$$

Hence, the equations that need to be solved are formulated in terms of a total and an incremental equation of equilibrium

$$\sum_i \left(\mathbf{a}^i\right)^T \mathbf{S}^i = \mathbf{R} \qquad (3\text{-}30)$$

$$\mathbf{K}_I(\mathbf{r})d\mathbf{r}=d\mathbf{R} \qquad (3\text{-}31)$$

For a given external load, **R** the displacement vector **r** is sought.
Various techniques for solving these non-linear problems exist. Herein three types of methods will be briefly described, namely:

- incremental or stepwise procedures(Euler-Cauchy method)
- iterative procedures (Newton-Raphson method)
- combined methods

In this paper, these methods are not considered, but the advanced solution is considered.

3.5.4 Advanced solution procedures

General

The solution procedure described so far are combination of incremental load coupled with full or modified Newton-Raphson iterations. Because the plastic flow rules are incremental in nature elasto-plastic problems should strictly be solved using small incremental steps. For, no matter how accurately flow rules and keeping on the yield surface may be satisfied within an increment, the solution is only in equilibrium at the end of each increment after equilibrium iterations. However, often acceptable solutions can be obtained with large steps.

Although incremental-iterative techniques provide the basis for most nonlinear finite element computer programs, additional sophistications are required to produce effective, robust solution algorithms. An extensive of more refined methods are discussed e.g. in Chapter 9 of Crisfield (1991). In this section a brief review of such methods is given.

In the present section emphasis will be placed on *arc-length techniques* for solving these problems. Prior to their introduction, analysts either used artificial springs, switched from load to displacement control or abandoning equilibrium iteration in the close vicinity of the limit point. In relation to structural analysis, the arc-length method was originally introduced by Riks [1972] and Wempner [1971] with later modifications being made by a number of authors.

The limit point represents the ultimate strength. There are several reasons:
i) In many cases it may be important to know not just the collapse load, but whether or not this collapse is of a “ductile” or “brittle “nature.
ii) The structure with the characteristic displayed in Fig. 12.22 may represent a component in structure. The ultimate behavior of a redundant structure consisting of such components would depend upon the post-ultimate beyond limit point, L) behavior of the component.

Method

As a starting point the global equilibrium equation is written as:

$$\mathbf{g}(\mathbf{r}, \lambda)=\mathbf{R}_{int}(\mathbf{r})-\lambda\mathbf{R}_{ref}=\mathbf{0} \qquad (3\text{-}32)$$

where $\mathbf{R}_{ref}$ is a fixed external load vector and the scalar λ is a load level parameter. Equation above defines a state of “*proportional loading*” in which the loading pattern is kept fixed. Non-proportional loading will be briefly mentioned later in this section.

The essence of the arc-length method is that the solution is viewed as the discovery of *a single equilibrium path* in a space defined by the nodal variables, **r** and the loading parameter, λ. Development of the solution requires a combined *incremental* (also called *predictor*) and *iterative* (also called *corrector*) approach.

Many of the materials (and possibly loadings) of interest will have path-dependent response. For these reasons, it is essential to limit the increment size. The increment size is limited by moving given distance along the tangent line to the current solution point and then searching for equilibrium in plane that passes through the point thus obtained and that is orthogonal to the same tangent line (Figure 3.8c).

In figure 3.8c the arc-length control strategies in the solution of nonlinear equations are illustrated and compared with load and displacement control. For instance if load incrementation is applied, the iterations are carried out to correct the displacements. When the arc-length method is applied the iterations are carried out with respect to both the load and displacements.

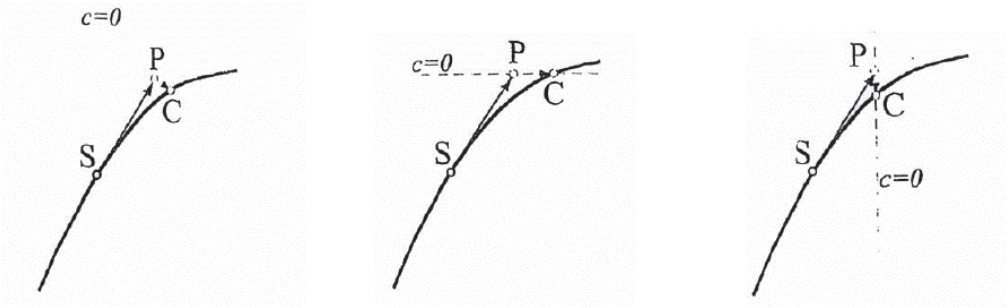

Figure 3.8Geometric representation of different control strategies of non-linear solution methods for single d.o.f.
a) Load control, b) state control, c) arc-length control

The arc length is formulated as an additional variable involving both the load and displacement. The increment in the load-displacement space can be described by a displacement vector $\Delta\mathbf{r}$ and a load increment parameter $\Delta\lambda$, such that $\Delta\mathbf{R} = \Delta\lambda\mathbf{R}_{ref.}$ This formulation results in an additional equation to be solved. The advantage of the extra equation is that the solution matrix never becomes 'singular' even at the limit points. Therefore, the solution matrix is re-assembled with N+ 1 variable, where N is the total number of the variables (degrees of freedom) of the system. However, the disadvantage is that the solution matrix becomes unsymmetric in some formulations, which may incur an increase in computing time and/or computer storage, particularly for very large problems. First the increment (predictor) from the "First point" is made along the tangent. Then, this solution is corrected iteratively to reach the "Second point" and so on.

Several methods exist to obtain the arc length, for example by making the iteration path follow a plane perpendicular to the tangent of the load-displacement curve, as shown in Figure 3.9. Alternatively, instead of a normal plane, more sophisticated paths such as spherical or cylindrical planes can be followed, and the solution matrix can be manipulated to become symmetric (see, for example, Crisfield [1991]).

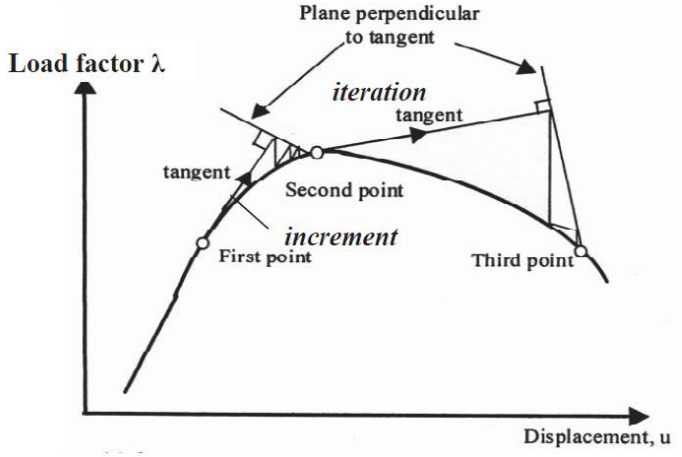

Figure 3.9: Schematic representation of the arc-length technique.

A geometrical interpretation of the incremental iterative approaches by Riks Wempner and Ramm is sketched in Figure 3.10. While in Ramm's method the iterative corrector is orthogonal to the current tangential plane during the iteration, it is orthogonal to the incremental vector $(\Delta r_0, \Delta r_0)$in the Riks-Wempner methods.

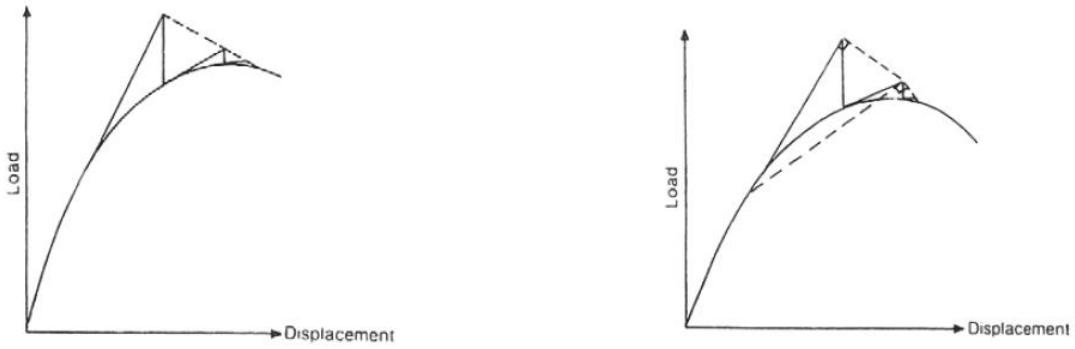

a) Riks-Wempner's method b) Ramm's method

Figure 3.10 Arc-length control methods (Crisfield, 1991)

An alternative iterative method is so-called orthogonal trajectory iterations (Fried, 1984). the first step in this method can be illustrated by reference to Figure 3.8. The first iteration is then assumed to be orthogonal to the vector S'P' instead of SP. The resulting iterative solution will appear as shown in Fig. 12.33.

Haugen (1994) found that this method was more efficient than the normal plane iterations.

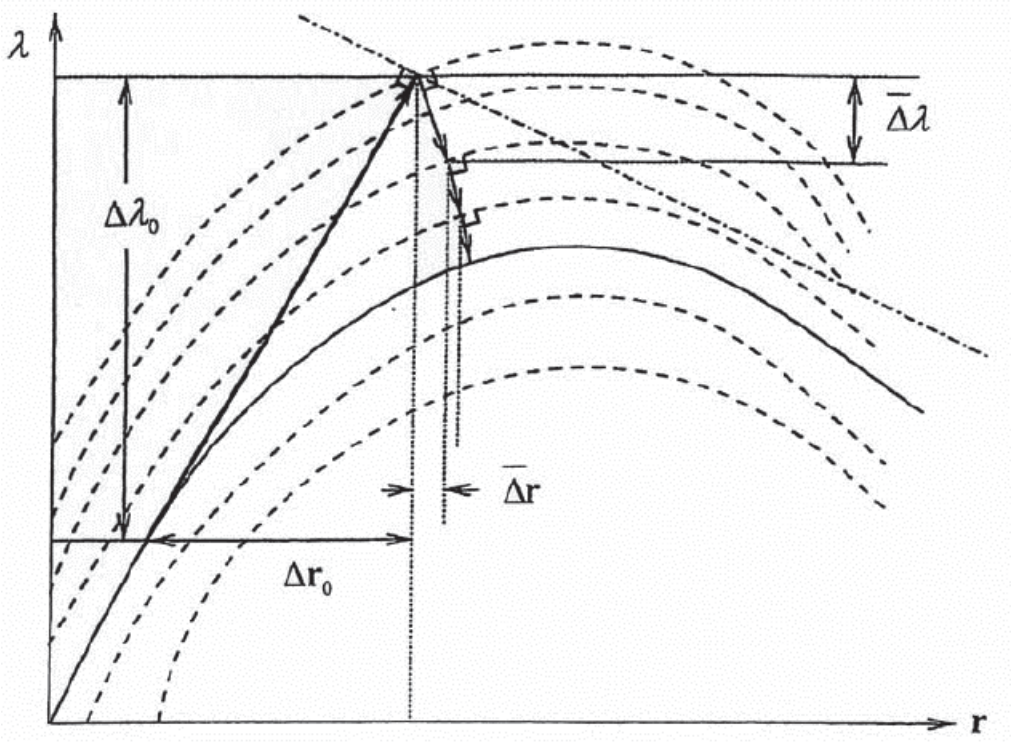

Figure 3.11 Arc-length method with orthogonal trajectory iterations.

Automatic incrementation

To achieve computational efficiency the load increment should be chosen depending upon the degree of nonlinearity of the problem. Methods have been established based on the curvature of the nonlinear path (den Heijer and Rheinboldt, 1981) or the so-called current stiffness parameter (Bergan et al, 1978):

$$S_p^i = \frac{\Delta r_1^T \Delta R_1}{\Delta \lambda_1^2} \frac{\Delta \lambda_i^2}{\Delta r_i^T \Delta R_i} \tag{3-33}$$

S_p^i refers to increment No.i.

The initial value of $S_p^i(S_p^1)$ is 1.0. For stiffening system it will increase. For softening system it will decrease. If S_p^ichanges sign the sign of the increment should be changed.

Numerical experiments show that nearly the same numbers of iterations are requested to restore equilibrium when the increments were chosen according to the approach of Bergan et al.(1978).

Ramm (1981) proposed another approach for estimating the necessary increment $\Delta\lambda$ (load incrementation) or $\Delta\lambda$ (for arc-length method). The new arc-length, l_n is obtained by

$$\Delta l_n = \Delta l_0 \left(\frac{I_d}{I_0}\right)^{1/2} \tag{3-34}$$

where Δ_0 is the "old" arc-length, and I_d and I_0 are the desired number of iterations

(given as input) and the number of iterations when the old arc-length was used. This approach requires a suitable estimate of the initial arc-length.

An alternative tactic is to apply load incrementation for early increments and switch to arc-length control once a limit point is approached.

The current stiffness parameter can be used to decide the switch from load incrementation (or displacement control) to the arc-length method. An alternative indicator of when the limit point is approached is the check of negative values on the diagonal of the incremental stiffness matrix, i.e. negative pivot elements in the solution algorithm.

In particular the current stiffness parameter may be used to control the solution strategy at limit points or bifurcation points. Alternative changes may be made when the current stiffness is below a limit value, namely

- the sign of the incrementation is changed
- iteration may be suppressed and a simple incrementation may be used. Iterations are then resumed when S_p^i increases beyond a specific limit (see Figure 3.12).

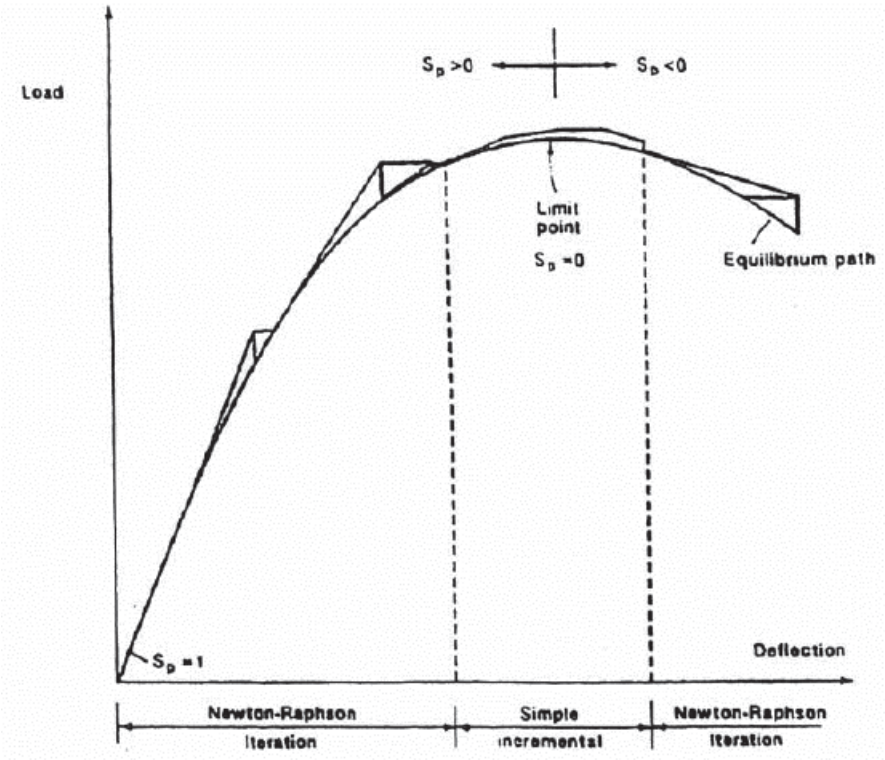

Figure 3.12 Possible choice of solution algorithm for a problem with limit point

Non-proportional loading

The solution procedures in this chapter have been based on the equilibrium

relationship of (12.101) which implies a single loading (or displacing) vector, $\mathbf{R}_{ref}$, is proportionally scaled via λ. For many practical structural problems, this loading regime is too restrictive. For example, we often wish to apply the "dead load" or "self-weight" and then monotonically increase the environmental load. Even more general load conditions may be required. Fortunately, many such loading regimes can be applied by means of a series of loading sequences involving two loading vectors, one that will be scaled (the previous $\mathbf{R}_{ref}$) and one that will be fixed $\mathbf{R}_{ref}$. The external loading can then be represented by

$$\mathbf{R}= \bar{\mathbf{R}}_{ref}+\lambda\, \mathbf{R}_{ref} \qquad (3\text{-}36)$$

so that the out-of-balance force vector becomes

$$g= \mathbf{R}_{int}-\bar{\mathbf{R}}_{ref}-\lambda\, \mathbf{R}_{ref} \qquad (3\text{-}37)$$

3.5.5 Direct integration methods

General

Up to now the methods for directly solving the statistic nonlinear equation have been based on incrementation of loads or displacements possibly combined with iterative methods. These are often considered standard methods for solving nonlinear problems (e.g. in ABAQUS).

An alternative approach is to use so-called finite difference methods for direct integration of the dynamic equation of motion:

$$\mathbf{M}\ddot{\mathbf{r}}(t)+\mathbf{C}\dot{\mathbf{r}}(t)+\mathbf{K}\mathbf{r}(t)=\mathbf{R}(t) \qquad (3\text{-}38)$$

to solve the static problem : $\mathbf{Kr}=\mathbf{R}$. Nonlinear structural effects make $\mathbf{K}$ a function of $\mathbf{r}$, $\mathbf{K}(\mathbf{r})$ .This means that the loading $\mathbf{R}$ is increased (artificially) or as a function of time. The loading time needs to be sufficiently long so that the inertia and damping forces do not have an effect on the behavior on the static problem that is to be solved.

A finite difference approximation is used when the time derivatives of (12.106) ($\ddot{\mathbf{r}}$ *and* $\dot{\mathbf{r}}$) are replaced by differences of displacement ($\mathbf{r}$) at various instants of time. The direct integration methods are alternatives to modal methods, and they can be used to successfully treat both geometric and material non-linearities. The finite difference methods are called *explicit* if the displacements at the new time step, $t+\Delta t$, can be obtained by the displacements, velocities and accelerations of previous time steps.

$$\mathbf{r}(t+\Delta t)=f\{\mathbf{r}(t),\dot{\mathbf{r}}(t),\ddot{\mathbf{r}}(t),\mathbf{r}(t-\Delta t),\dot{\mathbf{r}}(t-\Delta t),\ddot{\mathbf{r}}(t-\Delta t),\ldots\}$$

Or

$$\mathbf{r}_{i+1}=f\{\mathbf{r}_i,\dot{\mathbf{r}}_i,\ddot{\mathbf{r}}_i,\mathbf{r}_{i-1},\dot{\mathbf{r}}_{i-1},\ddot{\mathbf{r}}_{i-1},\ldots\} \qquad (3\text{-}39)$$

This is as opposed to the implicit finite difference formulations where displacements at the new time step $t+\Delta t$ are expressed by the velocities and accelerations at the new time step, in addition to the historical information at previous time steps.

$$\mathbf{r}_{i+1}=f\{\dot{\mathbf{r}}_{i+1},\ddot{\mathbf{r}}_{i+1},\mathbf{r}_i,\dot{\mathbf{r}}_i,\ddot{\mathbf{r}}_i,\ldots\}$$

Many of the implicit methods are unconditionally stable and the restrictions on the time step size are only due to requirements of accuracy. Explicit methods, on the other hand, are only stable for very short time steps.

Central difference method

To illustrate this approach, one of the explicit solution methods, the central difference method is described in the following. The central difference method is based on the assumption that the displacements at the new time step, $t+\Delta t$, and the previous time step, $t-\Delta t$, can be found by Taylor series expansion.

$$\mathbf{r}_{i+1}=\mathbf{r}_0(t)+\Delta t\dot{\mathbf{r}}_i+\frac{\Delta t^2}{2}\ddot{\mathbf{r}}_i+\frac{\Delta t^3}{6}\dddot{\mathbf{r}}_i+\ldots(\text{with } \mathbf{r}_0(t)=\mathbf{r}_i) \tag{3-40}$$

$$\mathbf{r}_{i-1}=\mathbf{r}_i-\Delta t\dot{\mathbf{r}}_i+\frac{\Delta t^2}{2}\ddot{\mathbf{r}}_i-\frac{\Delta t^3}{6}\dddot{\mathbf{r}}_i+\ldots \tag{3-41}$$

The terms with time steps to the power of three and higher are neglected. Subtracting Eq. (3-40) for Eq. (3-41) yields:

$$\mathbf{r}_{i+1}-\mathbf{r}_{i-1}=2\Delta t\dot{\mathbf{r}}_i \tag{3-42}$$

Adding Eq. (3-40,3-41) yields:

$$\mathbf{r}_{i+1}+\mathbf{r}_{i-1}=2\mathbf{r}+\Delta t^2\ddot{\mathbf{r}}_i \tag{3-43}$$

Rearranging Eq. (3-42, 3-43), the velocities and accelerations at the current time step can be expressed as:

$$\mathbf{r}_i=\frac{1}{2\Delta t}\{\mathbf{r}_{i+1}-\mathbf{r}_{i-1}\} \tag{3-44}$$

$$\ddot{\mathbf{r}}_i=\frac{1}{\Delta t^2}\{\mathbf{r}_{i+1}-2\mathbf{r}_i(t)+\mathbf{r}_{i-1}\} \tag{3-45}$$

Finally inserting Eqs. (3-44, 3-45) into the dynamic equation of motion gives:

$$\left\{\frac{1}{\Delta t^2}\mathbf{M}+\frac{1}{2\Delta t}\mathbf{C}\right\}\mathrm{r}_{i+1}=\mathbf{R}_i(t)-\mathbf{K}\mathbf{r}_i(t)+\frac{1}{\Delta t^2}\mathbf{M}\{2\mathbf{r}_i-\mathbf{r}_{i-1}\}+\frac{1}{2\Delta t}\mathbf{C}\mathbf{r}_{i-1} \tag{3-46}$$

If the mass matrix, $\boldsymbol{M}$, and the damping matrix, $\boldsymbol{C}$, are diagonal, the equations will be uncoupled, and the displacements at the next time step, $t+\Delta t$, can be optained without solving simultaneous equations.

The characteristic features of Eq. (3-46) are best illustrated by an example. Let us consider a system with three global directions of freedom. The mass matrix, $\mathbf{M}$ and damping matrix $\mathbf{C}$ are assumed to be diagonal.

Eq. (3-46) may then be written as:

$$\left\{\frac{1}{\Delta t^2}\begin{bmatrix}M_{11}&0&0\\0&M_{22}&0\\0&0&M_{33}\end{bmatrix}+\frac{1}{2\Delta t}\begin{bmatrix}C_{11}&0&0\\0&C_{22}&0\\0&0&C_{33}\end{bmatrix}\right\}\begin{bmatrix}r_{1(i+1)}\\r_{2(i+1)}\\r_{3(i+1)}\end{bmatrix}=\begin{bmatrix}R_{1(i)}\\R_{2(i)}\\R_{3(i)}\end{bmatrix}-\begin{bmatrix}K_{11}&K_{12}&K_{13}\\K_{21}&K_{22}&K_{23}\\K_{31}&K_{32}&K_{33}\end{bmatrix}\begin{bmatrix}r_{1(i)}\\r_{2(i)}\\r_{3(i)}\end{bmatrix}+$$

$$\frac{1}{\Delta t^2}\begin{bmatrix} M_{11} & 0 & 0 \\ 0 & M_{22} & 0 \\ 0 & 0 & M_{33} \end{bmatrix}\left\{ 2\begin{bmatrix} r_{1(i)} \\ r_{2(i)} \\ r_{3(i)} \end{bmatrix} - \begin{bmatrix} r_{1(i-1)} \\ r_{2(i-1)} \\ r_{3(i-1)} \end{bmatrix}\right\} + \frac{1}{2\Delta t}\begin{bmatrix} C_{11} & 0 & 0 \\ 0 & C_{22} & 0 \\ 0 & 0 & C_{33} \end{bmatrix}\begin{bmatrix} r_{1(i-1)} \\ r_{2(i-1)} \\ r_{3(i-1)} \end{bmatrix} \quad (3\text{-}47)$$

The first equation in Eq. (3-47) is explicitly written as:

$$\left\{\frac{1}{\Delta t^2}M_{11}+\frac{1}{2\Delta t}C_{11}\right\}r_{1(i+1)}=R_1(t)-K_{11}r_{1(i)}-K_{12}r_{2(i)}-K_{13}r_{3(i)}+\frac{1}{\Delta t^2}M_{11}\{2r_{1(i)}-r_{1(i-1)}\}+$$

$$\frac{1}{2\Delta t}C_{11}r_{1(i-1)} \quad (3\text{-}48)$$

This shows that $r_{i(i+1)}$ can be directly, explicity determined by the response at time t. There is no coupling between displacements, $r_{j(i+1)}$at the time $t+\Delta t$.

Because the expressions for the displacements are explicitly given, there is no need to invert the tangent stiffness matrix at every time step. The explicit method also has the advantage of drastically reducing the need for computer memory capacity. The stiffness forces, or internal force vector, can be found by summation of element contributions. The global stiffness vector, ***K*,** need not to be stored in the computers core memory.

As already mentioned, Eq. (3-49) is conditionally stable and requires that

$$\Delta t<\frac{2}{\omega_{max}} \quad (3\text{-}49)$$

where ω_{max} is the highest natural frequency of

$$\det(\mathbf{K}-\omega^2\mathbf{M})=0 \quad (3\text{-}50)$$

The maximum frequency of Eq. (3-50) is bounded by the maximum frequency of the constituent unassembled and unsupported elements. When finding the maximum natural frequency of an element, one will see that the time step, Δt, must be short enough that information does not propagate across more than one element per time step. The maximum allowable time step will therefore be limited by a characteristic length, λ_e, of the element and the acoustic wave speed, c.

$$\Delta t<\frac{\lambda_e}{c}$$

Higher order elements yield higher maximum frequencies and should be avoided when doing explicit integration. Many alternative methods exist.

Solution of static problems

The explicit method is very well suited to treat dynamic problems. As indicated above the method can also be used to solve static problems.

It is obvious that the period of the loading, or the amount of time for the loading to reach its maximum value, must be much larger than the largest Eigen period to avoid dynamic effects as determined from the lowest Eigen frequency found for Eq.(3-50).

The response of the structure is also dependent on the magnitude of the loading, not only on the period, and this complicates the picture. In addition, failures due to collapse or cracking of parts of the structure will cause vibrations. These events will not be captured by a traditional static analysis.

All effects taken into account; if the time of the loading to reach its maximum level is conservatively chosen to be 30 times the longest Eigen period of the system, the dynamic effects have shown to be negligible.

Another problem with explicit analyses is that post-collapse behavior cannot be traced if the loading is given as applied forces. In many cases this can be avoided by switching to displacement control. If displacement control is not possible or desirable, implicit solution procedures using arc length solution methods can be used.

An advantage with the explicit solution procedure is that it is very easy to use. The user of an explicit finite element program is left with the difficulty of applying loads sufficiently slowly to avoid dynamic phenomena and sufficiently fast to avoid too large computational efforts times.
In static analyses, and even in dynamic analyses, the computational time van be considerably reduced by changing mass densities in elements. The time step will be governed by the smallest element in the model. Artificially increasing the mass of small elements will reduce the acoustic wave speed and hence allow longer time steps. Similarly very large elements can be given mass reduction and hence be less affected by inertia forces. Systematic increase and reduction of element masses can be performed to improve computational efficiency, but the details in these methods will not be elaborated on.

3.6 Introduction to riks method in ABAQUS[35]

During the preparation when studying ABAQUS, a lot of documents are read. In order to perform the post-buckling analysis, the method of riks needs to be used.

The Riks method:

- is generally used to predict unstable, geometrically nonlinear collapse of a structure
- can include nonlinear materials and boundary conditions;
- often follows an eigenvalue buckling analysis to provide complete information about a structure's collapse;
- can be used to speed convergence of ill-conditioned or snap-through problems that do not exhibit instability.

3.6.1 Unstable response

Geometrically nonlinear static problems sometimes involve buckling or collapse behavior, where the load-displacement response shows a negative stiffness and the structure must release strain energy to remain in equilibrium. Several approaches are possible for modeling such behavior. One is to treat the buckling response dynamically, thus actually modeling the response with inertia effects included as the structure snaps. This approach is easily accomplished by restarting the terminated static procedure and switching to a dynamic procedure when the static solution becomes unstable. In some simple cases displacement control can provide a solution, even when the conjugate load (the reaction force) is decreasing as the displacement increases. Another approach would be to use dashpots to stabilize the structure during a static analysis. Abaqus/Standard offers an automated version of this stabilization approach for the static analysis procedures.

Alternatively, static equilibrium states during the unstable phase of the response can be found by using the "modified Riks method." This method is used for cases where the loading is proportional; that is, where the load magnitudes are governed by a single scalar parameter. The method can provide solutions even in cases of complex, unstable response such as that shown in Figure 3.13.

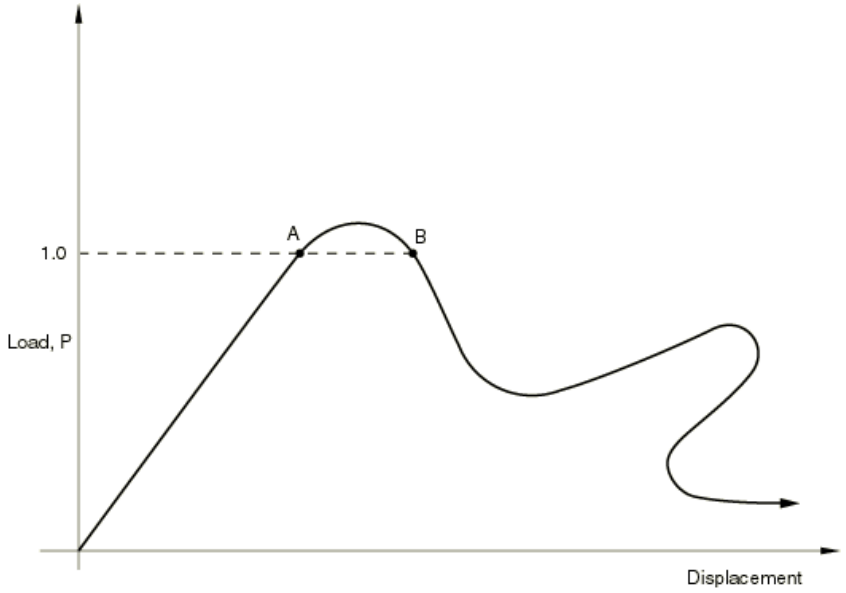

Figure 3.13 complex, unstable response

The Riks method is also useful for solving ill-conditioned problems such as limit load problems or almost unstable problems that exhibit softening.

In simple cases linear eigenvalue analysis ("Eigenvalue buckling prediction,")may be sufficient for design evaluation; but if there is concern about material nonlinearity, geometric nonlinearity prior to buckling, or unstable postbuckling response, a load-deflection (Riks) analysis must be performed to investigate the problem further.

The Riks method uses the load magnitude as an additional unknown; it solves simultaneously for loads and displacements. Therefore, another quantity must be used to measure the progress of the solution; Abaqus/Standard uses the "arc length," l, along the static equilibrium path in load-displacement space. This approach provides solutions regardless of whether the response is stable or unstable.

3.6.2 Proportional loading

If the Riks step is a continuation of a previous history, any loads that exist at the beginning of the step and are not redefined are treated as "dead" loads with constant magnitude. A load whose magnitude is defined in the Riks step is referred to as a "reference" load. All prescribed loads are ramped from the initial (dead load) value to the reference values specified.

The loading during a Riks step is always proportional. The current load magnitude, , is defined by

$P_{total}=P_0+\lambda(P_{ref}-P_0)$

Where P_0 is the "dead load," P_{ref} is the reference load vector, and λ is the "load proportionality factor." The load proportionality factor is found as part of the solution. Abaqus/Standard prints out the current value of the load proportionality factor at each increment.

3.6.3 Incrementation

Abaqus/Standard uses Newton's method to solve the nonlinear equilibrium equations. The Riks procedure uses only a 1% extrapolation of the strain increment.

You provide an initial increment in arc length along the static equilibrium path Δl_{in}, when you define the step. The initial load proportionality factor, $\Delta\lambda_{in}$, is computed as

$$\Delta\lambda_{in}=\frac{\Delta l_{in}}{l_{period}}$$

Where l_{period} is a user-specified total arc length scale factor (typically set equal to 1). This value of $\Delta\lambda_{in}$ is used during the first iteration of a Riks step. For subsequent iterations and increments the value of λ is computed automatically, so you have no control over the load magnitude. The value of λ is part of the solution. Minimum and maximum arc length increments, Δl_{min} and Δl_{max}, can be used to control the automatic incrementation.

3.6.4 Input File Usage:

*STATIC, RIKS
Abaqus/CAE Usage:
Step module: Create Step: General: Static, Riks
Direct user control of the increment size is also provided; in this case the incremental arc length is kept constant. This method is not recommended for a Riks analysis since it prevents Abaqus/Standard from reducing the arc length when a severe nonlinearity is encountered.
Input File Usage:
*STATIC, RIKS, DIRECT
Abaqus/CAE Usage:
Step module: Create Step: General: Static, Riks: Incrementation: Type: Fixed
Ending a Riks analysis step
Since the loading magnitude is part of the solution, you need a method to specify when the step is completed. You can specify a maximum value of the load proportionality factor, or a maximum displacement value at a specified degree of freedom. The step will terminate when either value is crossed. If neither of these finishing conditions is specified, the analysis will continue for the number of increments specified in the step definition.

3.6.5 Bifurcation

The Riks method works well in snap-through problems—those in which the equilibrium path in load-displacement space is smooth and does not branch. Generally you do not need take any special precautions in problems that do not exhibit branching (bifurcation). “Snap-through buckling analysis of circular arches,” Section 1.2.1 of the Abaqus Example Problems Manual, is an example of a smooth snap-through problem.
The Riks method can also be used to solve postbuckling problems, both with stable and unstable postbuckling behavior. However, the exact postbuckling problem cannot be analyzed directly due to the discontinuous response at the point of buckling. To analyze a postbuckling problem, it must be turned into a problem with continuous response instead of bifurcation. This effect can be accomplished by introducing an initial imperfection into a “perfect” geometry so that there is some response in the buckling mode before the critical load is reached.

3.6.6 Introducing geometric imperfections

Imperfections are usually introduced by perturbations in the geometry. Unless the precise shape of an imperfection is known, an imperfection consisting of multiple superimposed buckling modes must be introduced ("Eigenvalue buckling prediction,"). Abaqus allows you to define imperfections; see "Introducing a geometric imperfection into a model," Section 11.3.1.

In this way the Riks method can be used to perform postbuckling analyses of structures that show linear behavior prior to (bifurcation) buckling. An example of this method of introducing geometric imperfections is presented in "Buckling of a cylindrical shell under uniform axial pressure".

By performing a load-displacement analysis, other important nonlinear effects, such as material inelasticity or contact, can be included. In contrast, all inelastic effects are ignored in a linear eigenvalue buckling analysis and all contact conditions are fixed in the base state. Imperfections based on linear buckling modes can also be useful for the analysis of structures that behave inelastically prior to reaching peak load.

3.6.7 Introducing loading imperfections

Perturbations in loads or boundary conditions can also be used to introduce initial imperfections. In this case fictitious "trigger" loads can be used to initiate the instability. The trigger loads should perturb the structure in the expected buckling modes. Typically, these loads are applied as dead loads prior to the Riks step so that they have fixed magnitudes. The magnitudes of trigger loads must be sufficiently small so that they do not affect the overall postbuckling solution. It is your responsibility to choose appropriate magnitudes and locations for such fictitious loads; Abaqus/Standard does not check that they are reasonable.

3.6.8 Obtaining a solution at a particular load or displacement value

The Riks algorithm cannot obtain a solution at a given load or displacement value since these are treated as unknowns—termination occurs at the first solution that satisfies the step termination criterion. To obtain solutions at exact values of load or displacement, the solution must be restarted at the desired point in the step

("Restarting an analysis") and a new, non-Riks step must be defined. Since the subsequent step is a continuation of the Riks analysis, the load magnitude in that step must be given appropriately so that the step begins with the loading continuing to increase or decrease according to its behavior at the point of restart. For example, if the load was increasing at the restart point and was positive, a larger load magnitude than the current magnitude should be given in the restart step to continue this behavior. If the load was decreasing but positive, a smaller magnitude than the current magnitude should be specified.

3.6.9 Restrictions

1. A Riks analysis is subject to the following restrictions:

2. A Riks step cannot be followed by another step in the same analysis. Subsequent steps must be analyzed by using the restart capability.

3. If a Riks analysis includes irreversible deformation such as plasticity and a restart using another Riks step is attempted while the magnitude of the load on the structure is decreasing, Abaqus/Standard will find the elastic unloading solution. Therefore, restart should occur at a point in the analysis where the load magnitude is increasing if plasticity is present.

4. For postbuckling problems involving loss of contact, the Riks method will usually not work; inertia or viscous damping forces (such as those provided by dashpots) must be introduced in a dynamic or static analysis to stabilize the solution.

3.6.10 Abaqus settings.

1. Initial conditions
Initial values of stresses, temperatures, field variables, solution-dependent state variables, etc. can be specified; "Initial conditions in Abaqus/Standard and Abaqus/Explicit," Section 32.2.1, describes all of the available initial conditions.

2. Boundary conditions
Boundary conditions can be applied to any of the displacement or rotation degrees of freedom (1–6) or to warping degree of freedom 7 in open-section beam elements Amplitude definitions cannot be used to vary the magnitudes of prescribed boundary conditions during a Riks analysis.

3.Loads

The following loads can be prescribed in a Riks analysis:
Concentrated nodal forces can be applied to the displacement degrees of freedom (1–6);

Distributed pressure forces or body forces can be applied; see "Distributed loads," Section 32.4.3. The distributed load types available with particular elements are described in Part VI, "Elements."

Since Abaqus/Standard scales loading magnitudes proportionally based on the user-specified magnitudes, amplitude references are ignored when the Riks method is chosen.

If follower loads are prescribed, their contribution to the stiffness matrix may be unsymmetric; the unsymmetric matrix storage and solution scheme can be used to improve computational efficiency in such cases.

4. Predefined fields
Nodal temperatures can be specified (see "Predefined fields," Section 32.6.1). Any difference between the applied and initial temperatures will cause thermal strain if a thermal expansion coefficient is given for the material ("Thermal expansion," Section 25.1.2). The loads generated by the thermal strain contribute to the "reference" load specified for the Riks analysis and are ramped up with the load proportionality factor. Hence, the Riks procedure can analyze postbuckling and collapse due to thermal straining.

The values of other user-defined field variables can be specified. These values affect only field-variable-dependent material properties, if any. Since the concept of time is replaced by arc length in a Riks analysis, the use of properties that change due to changes in temperatures and/or field variables is not recommended.

5. Material options
Most material models that describe mechanical behavior are available for use in a Riks analysis. The following material properties are not active during a Riks analysis: acoustic properties, thermal properties (except for thermal expansion), mass diffusion properties, electrical properties, and pore fluid flow properties. Materials with history dependence can be used; however, it should be realized that the results will depend on the loading history, which is not known in advance.

The concept of time is replaced by arc length in a Riks analysis. Therefore, any effects involving time or strain rate (such as viscous damping or rate-dependent plasticity) are no longer treated correctly and should not be used.

6. Elements

Any of the stress/displacement elements in Abaqus/Standard (including those with temperature or pressure degrees of freedom) can be used in a Riks analysis (see "Choosing the appropriate element for an analysis type," Section 26.1.3). Dashpots should not be used since velocities will be calculated as displacement increments divided by arc length, which is meaningless.

7. Output

Output options are provided to allow the magnitudes of individual load components (pressure, point loads, etc.) to be printed or to be written to the results file. The current value of the load proportionality factor, LPF, will be given automatically with any results or output database file output request. These output options are recommended when the Riks method is used so that load magnitudes can be seen directly. All of the output variable identifiers are outlined in "Abaqus/Standard output variable identifiers," Section 4.2.1.

4. Numerical model and validation

In this chapter, X-joint models are mainly studied. BOMEL X-braced Frame II[5] was chosen to build the X-joint model (168OD×5.1DT). The X-joints will be modeled singly and as a part of a frame. For the isolated joint models, 3 load cases are considered. During the study, it is found that the X-joint's brace which is in compression is more critical under large load, and when in frame it shows the similar features. Also critical strain is discussed.

4.1 Review of the specialization project

4.1.1 Model Generation

In the specialization project, in order to perform a simulation of an X-joint with ABAQUS, and the length of the brace is decided to be 5 times as the outer diameter (840mm).

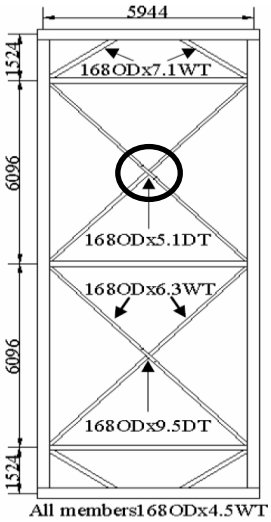

Figure 4.1The joint chosen for building model

As ABAQUS is not the professional software for generating models, PATRAN is recommended to generate the model. The X-joint is divided into 4 parts by the intersection in the middle. So it is needed to connect the parts after importing into ABAQUS. However the effect is not very satisfactory. Mesh near the intersection cannot be aligned due to insufficient accuracy. Thus software HyperMesh is then needed to draw mesh on the surface. Then the four parts become one assembly. Figure 4.2 shows interface of HyperMesh.

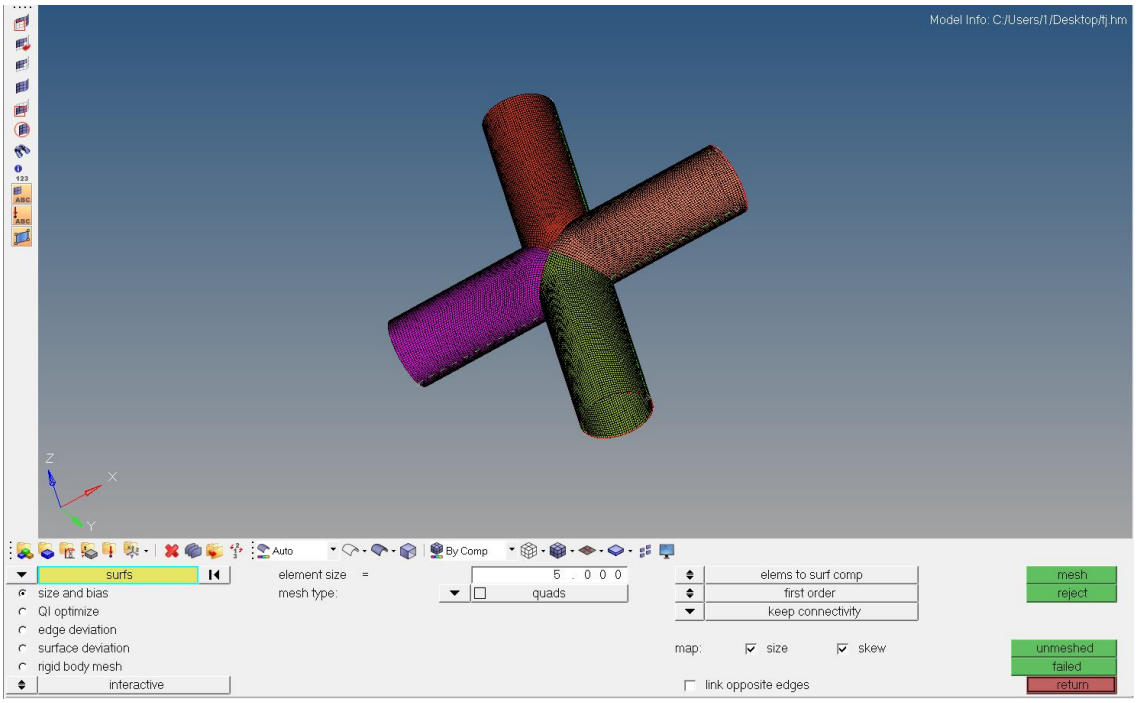

Figure 4.2 Auto-meshing the joint by using HyperMesh

After Hypermesh, the four separate parts become together as one part, the intersection places are connected well to each other. Now it can be imported to ABAQUS for doing the analysis.

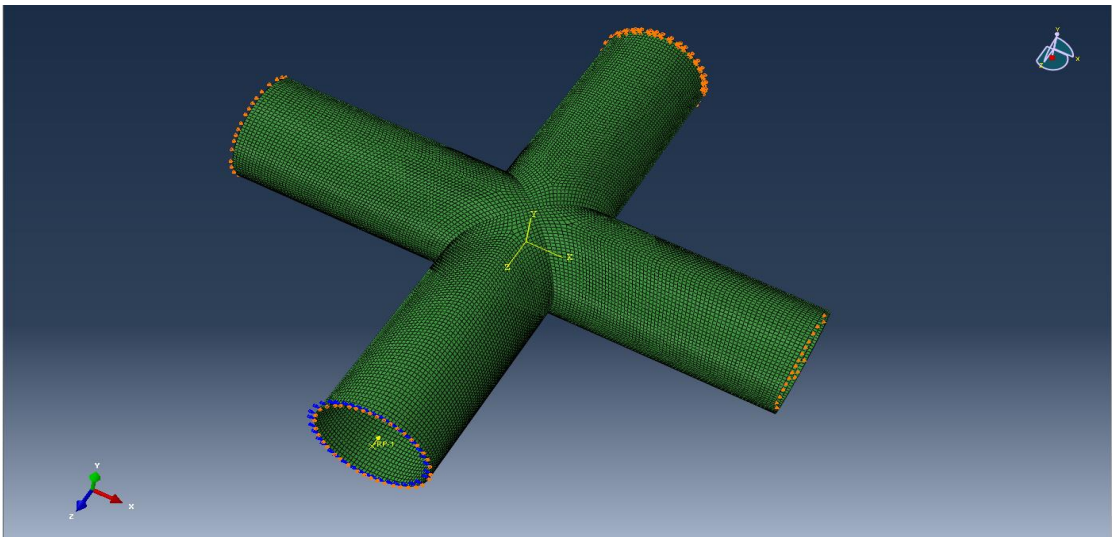

Figure 4.3 Mesh and model in ABAQUS

Three load cases are to be used which is shown in Figure 4.4

N_1 is compression force and N_2 is tension force.

Load case 1: $N_2=0$,

Load case 2: $N_2=N_1$

Load case 3: $N_2=0.5N_1$

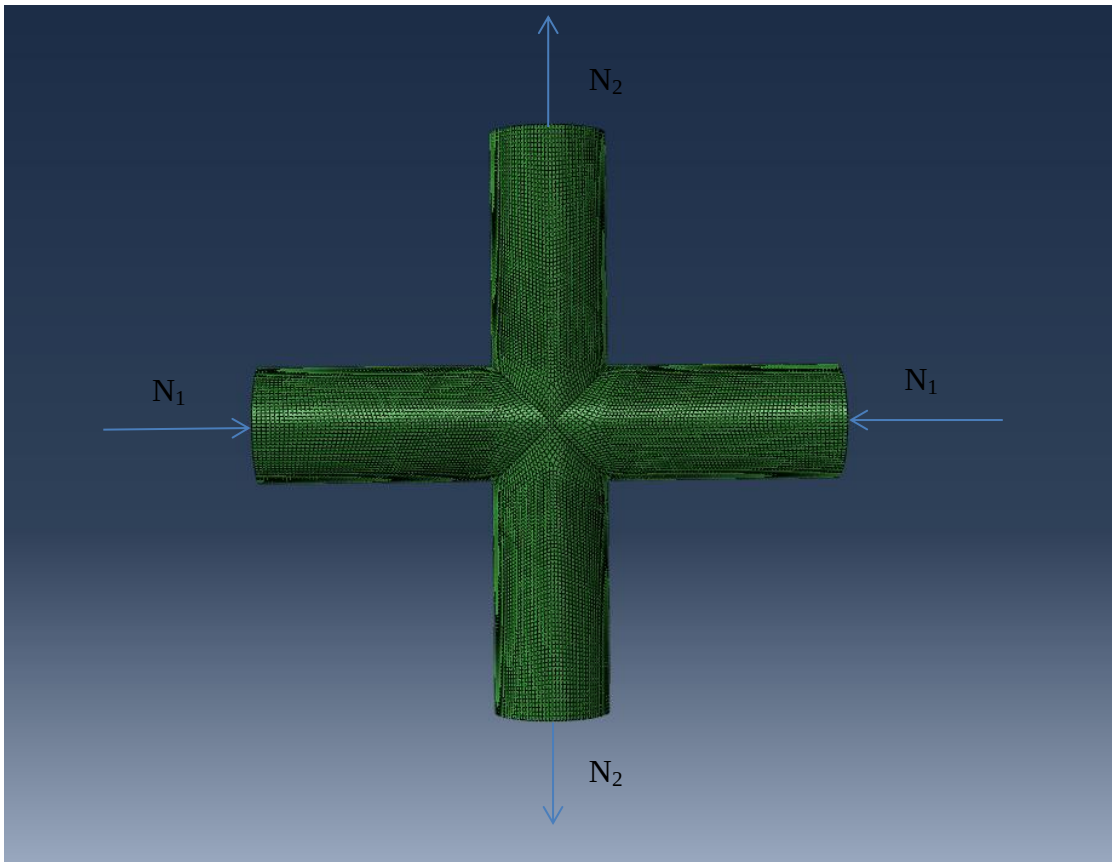

Figure 4.4 Load distributions on the joint

4.1.2 Analysis results

First axial resistance defined by Norsok-004 is calculated by using the formulations mentioned in Chapter 2.

The above geometry parameters of the model:

$\beta=1,\ \gamma=\frac{168}{10.2}=16.47,\ \tau=1,\ \alpha=\frac{2L}{D}=10,\ f_y=345N/mm^2$

$N_{Rd}=\frac{f_y T^2}{\gamma_M \sin\theta} Q_u Q_f=\frac{345\times5.1^2}{1.15\times1} Q_u Q_f$

$Q_\beta=\frac{0.3}{\beta(1-0.833\beta)}=\frac{0.3}{0.167}=1.7964$

$Q_u=(2.8+14\beta)Q_\beta=16.8\times1.7964=30.17952$

$A=C_1\left(\frac{\sigma_{a,Sd}}{f_y}\right)^2+C_2\left(\frac{\sigma_{my,Sd}^2+\sigma_{mz,Sd}^2}{1.62f_y^2}\right)=20\times\left(\frac{200}{345}\right)^2+22\times\left(\frac{150^2\times2}{1.62\times345^2}\right)=11.854$

$Q_f=1.0$

$$N_{Rd}=\frac{f_y T^2}{\gamma_M \sin\theta} Q_u Q_f=\frac{345\times 5.1^2}{1.0\times 1} Q_u Q_f=270814.4N$$

Estimated values are made for $\sigma_{my,Sd}$ and $\sigma_{mz,Sd}$.

The history output is set to displacement of the reference point and Load proportional factor. The displacement-load curves are plotted after the calculation. The force-deformation behaviour of the joint in different cases is shown in Fig. 4.5.

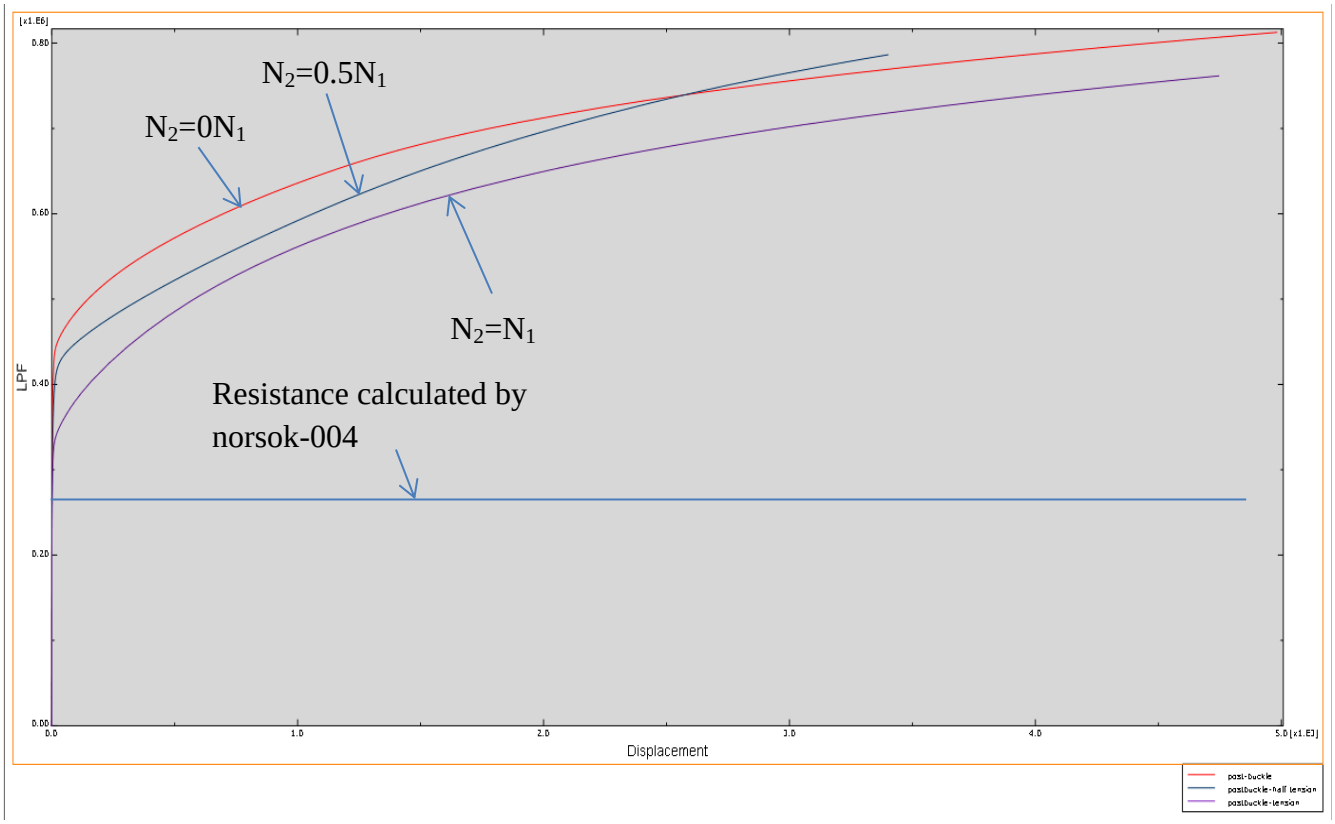

Figure 4.5 Displacement-LPF curves

From Figure 4.5 we can see that the curves' tendencies are similar: at the first stage displacement changes little while the LPF rises sharply, and then the slope of the curves become smaller. At the end the slope becomes near to zero, i.e. the displacement is increasing while the LPF doesn't change much, which corresponds to the plastic deformation. Also the figure indicates the comparison with resistance calculated by Norsok004. We can see that the Norsork004 resistance is much smaller than the magnitude of the inflection point of the curves, which indicates that the code calculated values are conservative. More reasonable measures may be recommended.

The three curves are compared also. From Figure 4.5 we can see the capacity of the joints is more sufficient when no axial tension load is applied on them. When axial tension load is added to the joints, the LPF is smaller at the same displacement than the one without tension load. The larger the tension load is, the less sufficient capacity the joints show.

However, the curves obtained are not so satisfactory because the curve is always on the rise without descent stage, which is inconsistent with the actual reality.

4.2 Work in master thesis

In the master thesis project, a lot more work has been done for this joint model. And the curves obtained in specialization project are proved to be not so correct, though deformation type is similar with the experimental test. The major reason of this is due to non-linear effects not taken into account.

4.2.1 The application of Riks method

The line-perturbation is the eigenvalue analysis of buckling. It is a linear analysis, while non-linear buckling analysis is to be performed. In order to do so, initial imperfection is to be imported.

ABAQUS has three methods to identify initial imperfection: taking a linear combination of the branch buckling model, taking the results based on static analysis, specifying directly. The first method is normally used, and the procedures are as follows:

1. Write the eigenmodes in the default global system to the results file as nodal data
2. Add the eigenmodes to the perfect geometry as the initial imperfection, and the associated scale factor is largest in the 1st modeshape. The scale factor is usually taken as the multiple of the geometry parameters, for example, 0.1 times of the shell thickness, etc.
3. Analyze by using the riks method.

Defining an imperfection based on eigenmode data
Input File Usage:
*IMPERFECTION, FILE=results file, STEP=step, NSET=name
Defining an imperfection based on static analysis data
In order to use the eigenvalue file, the model keywords of the buckle is to be modified.
*node file,
*u
Add these two sentences to the keywords. The location is shown in figure below.

```
*Restart, write, frequency=0
*nodefile
u,
**
** FIELD OUTPUT: F-Output-1
**
*Output, field, variable=PRESELECT
```

4.2.2 Model generation

First, the material is optimized by adding hardening area in order to make it closer to the reality.

The yield criterion states that yielding begins when stress reaches yield stress, in practice usually taken as the tensile yield strength. Subsequent plastic deformation may alter the stress needed to produce renewed or continued yielding

	Yield Stress	Plastic Strain
1	355	0
2	410	0.05
3	450	0.1
4	480	0.15

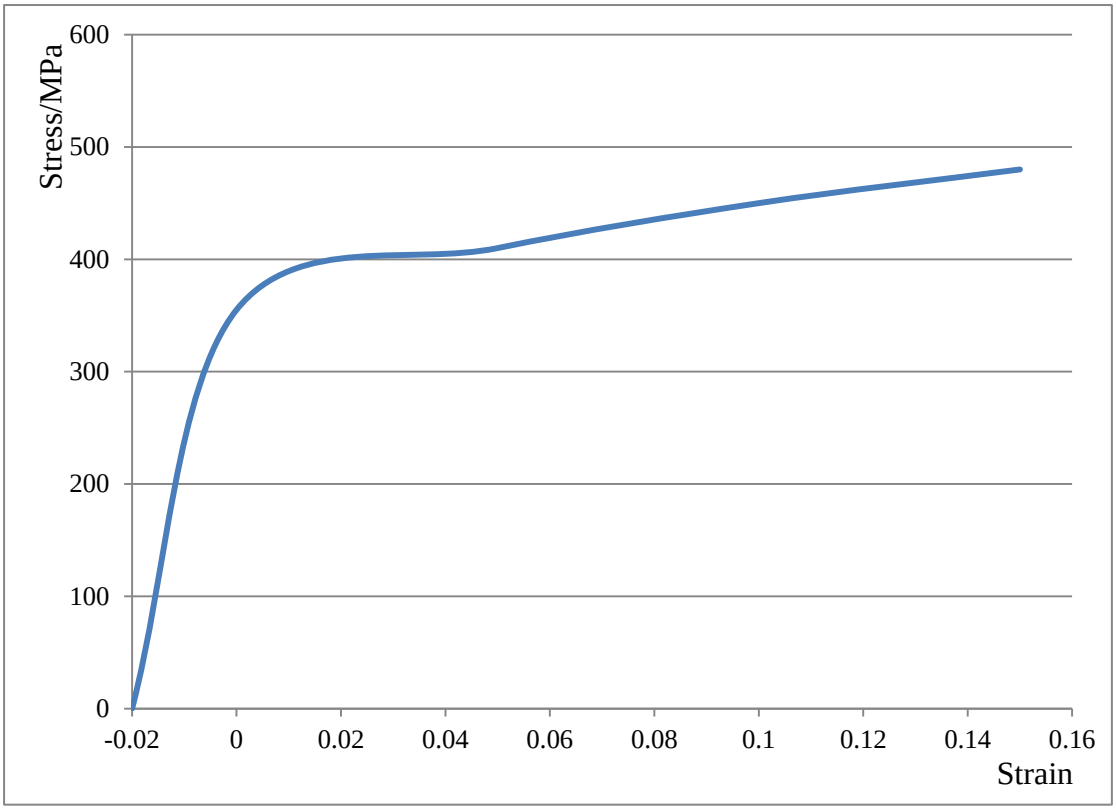

Figure 4.6 Material stress and strain relation curve

As required in the master thesis task, analysis is to be performed with single joints and

joints as a part of a frame system plane frame system, so a model of single joint as a part of a frame system is built as shown in Figure 4.7. And a push-over analysis is to be performed.

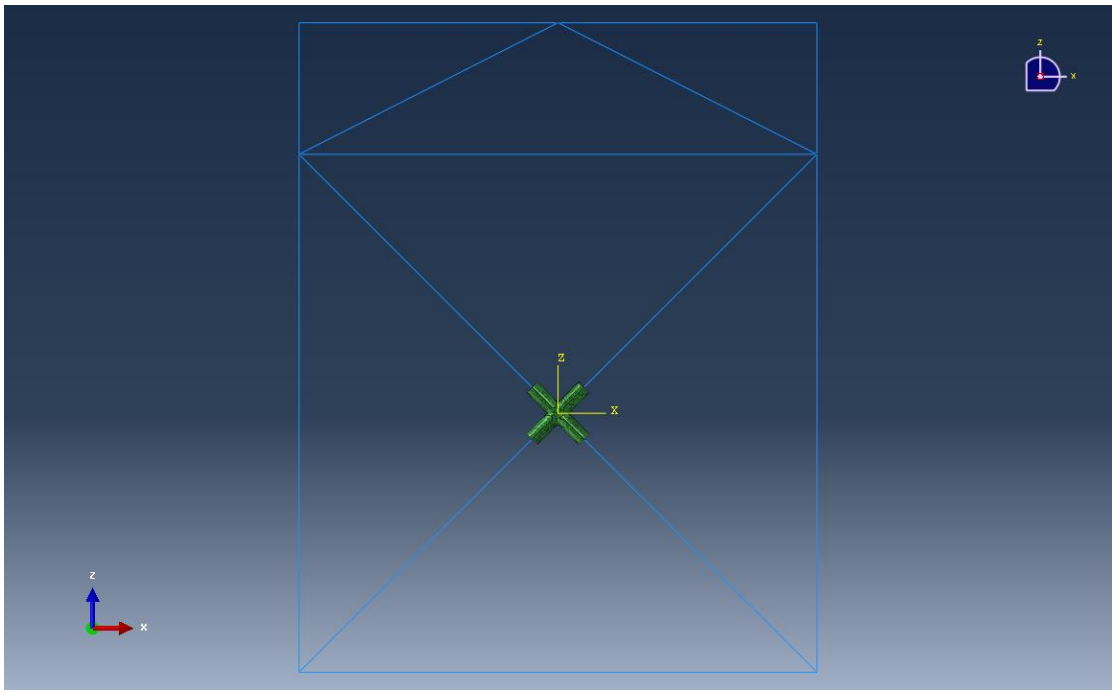

Figure 4.7 Single joint as a part of a frame system

The dimension of the frame are shown in Figure 4.8

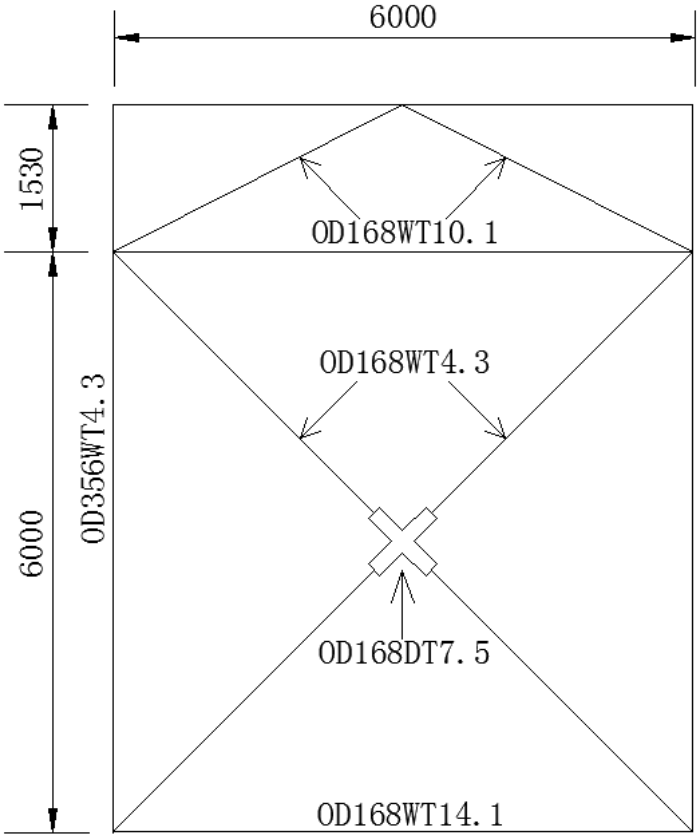

Figure 4.8 Dimension

The constraint type of coupling is used as the interaction between the frame edges and the joint (See Figure 4.9).

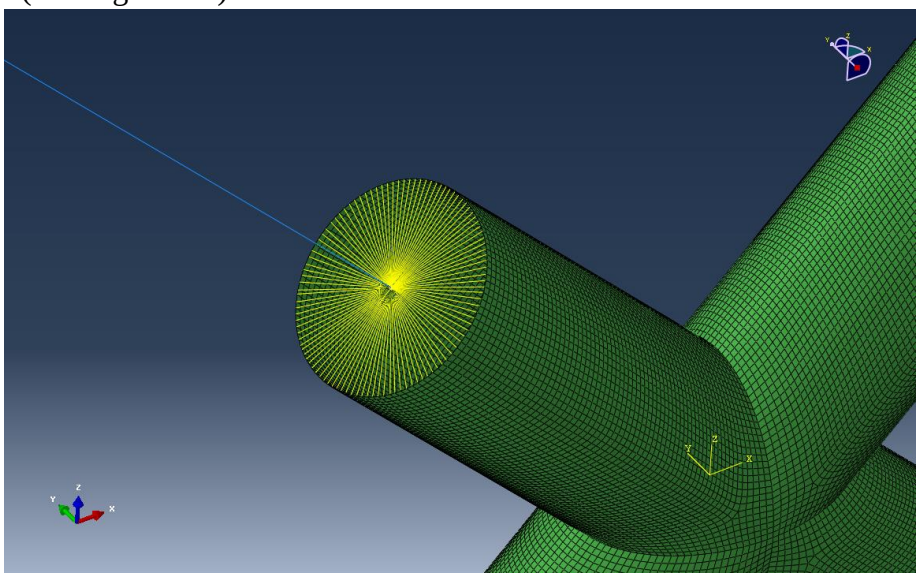

Figure 4.9 Interaction used between frame and joint

In reality, a through member is usually used when a joint is built by the same method mentioned, i.e. the joint consists of a through member and two separate braces welded to the through member, which is shown in Figure 4.10.

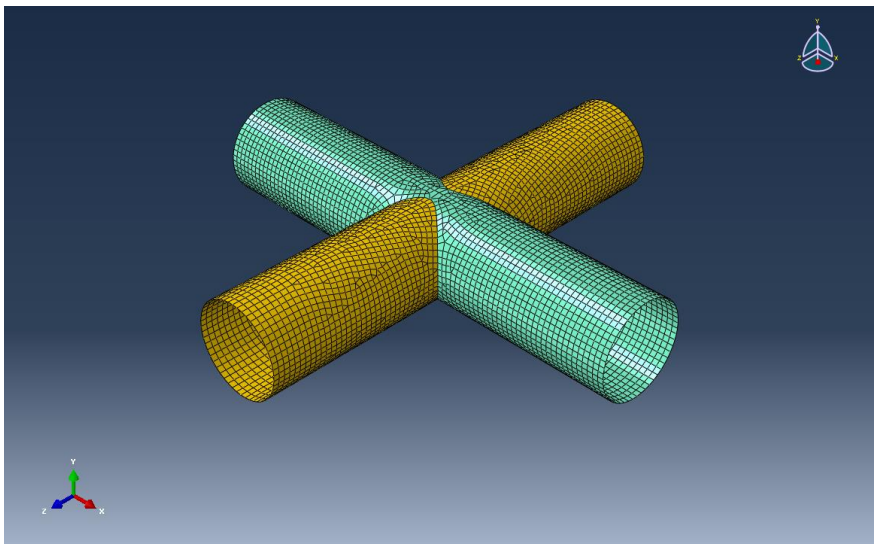

Figure 4.10 new joint model with a through member

Similarly, a model of this single joint as a part of a frame system is built with the same dimension.

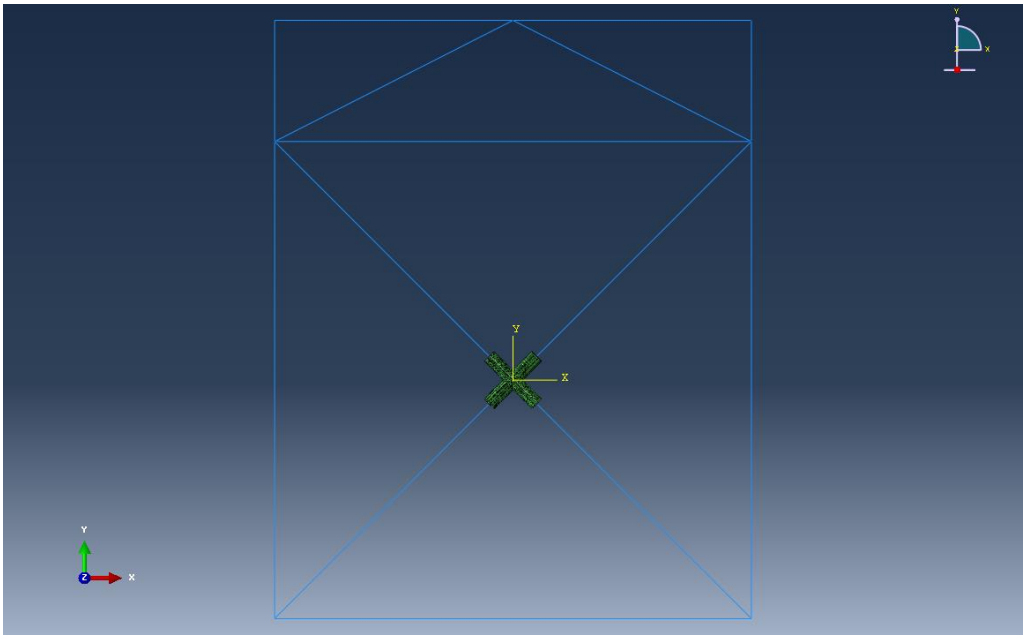

Figure 4.11 single joint as a part of a frame system (new)

4.2.3 Analysis results

Different sets are made to record the change of variables, the comparison of which are shown in figures below.

1) Improved curve of force-deformation relationship of the old single joint model

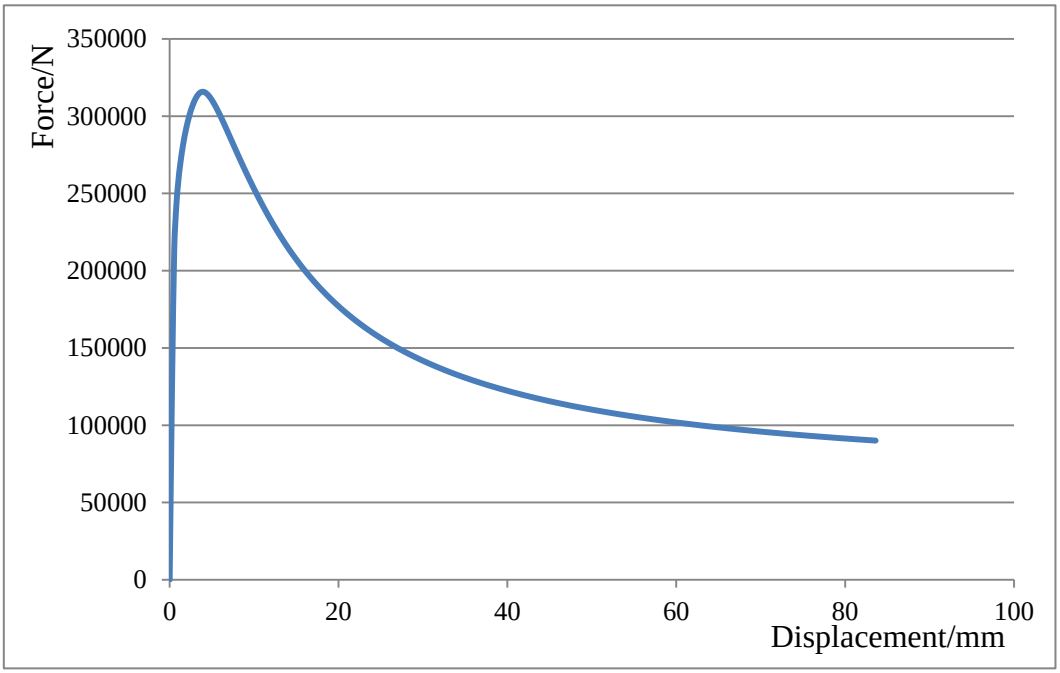

Figure 4.12 Improved curve of force-deformation relationship of the old single joint model

From the figure it is seen that the curve has a significant declining segment, which is totally different from the curve obtained in specialization project. The force rises

sharply at the first stage until it reaches the critical load, after which it declined rapidly with the increase of the displacement. The difference can be explained by whether non-linear effects are taken into account or not, which, in ABAQUS, is reflected by choosing nlgeom or not (geometry in non-linear).

The deformation and plot of stresses of the joint in different stages are shown in Figure 4.13.

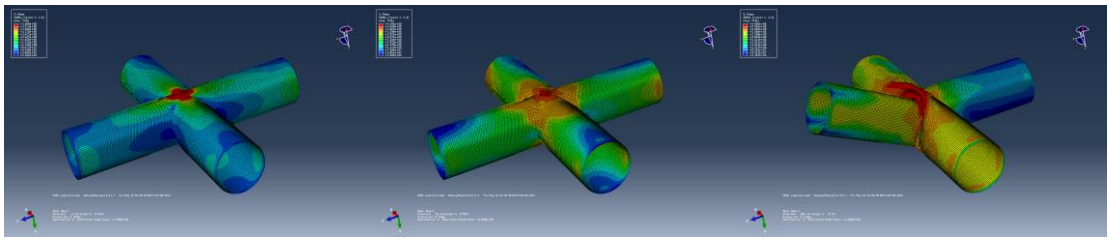

Figure 4.13 the deformation and plot of stresses of the joint in different stages

As shown in the figure 4.13, the joint has a very obvious buckling, as the compression brace warps and compresses the tension braces.

2) The curve of force-deformation relationship of the new single joint model

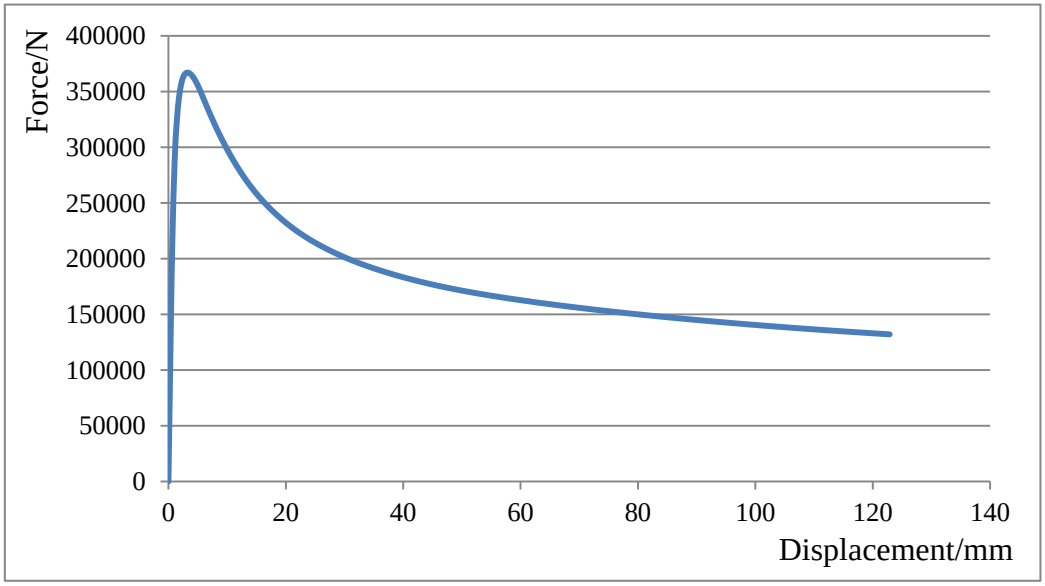

Figure 4.14 the curve of force-deformation relationship of the new single joint model

The curve of force-deformation relationship of the new single joint model shows the same trend as the old single one, also the deformation and plot of stresses of the joint in different stages.

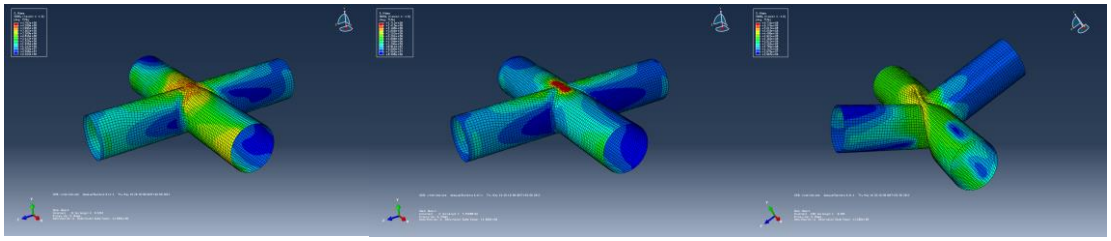

Figure 4.15 the deformation and plot of stresses of the joint in different stages

3) Comparison of the two curves of the two different models.

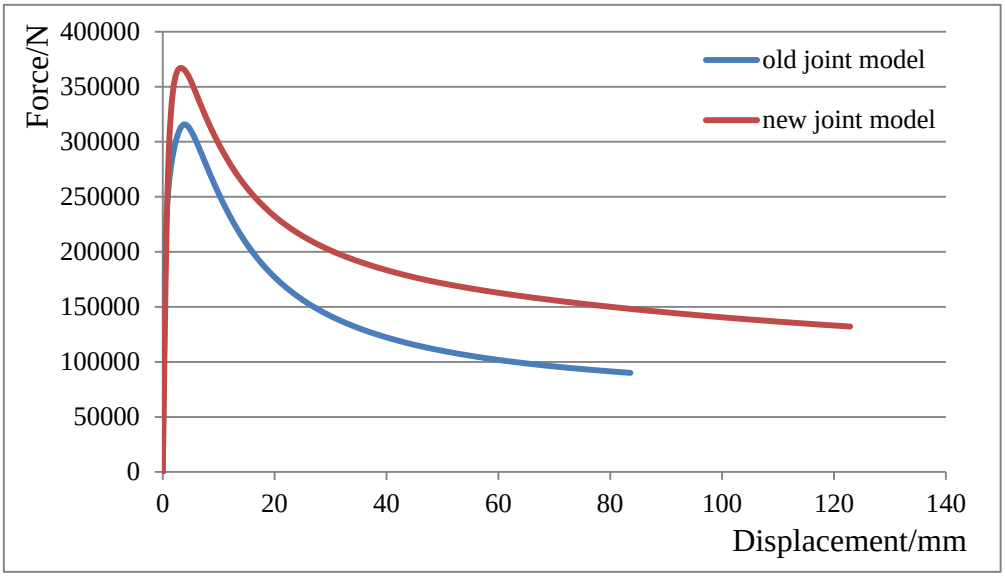

Figure 4.16 Comparison of the force-displacement relation curve of the old and new joint model

From the figure it is seen that the new joint model has a larger critical load than the old one, which proves that the through member makes a contribution to the capacity of the joints.

4) The old single joint as a part of a frame system

The LPF and global displacement relation curve is shown in Figure 4.17

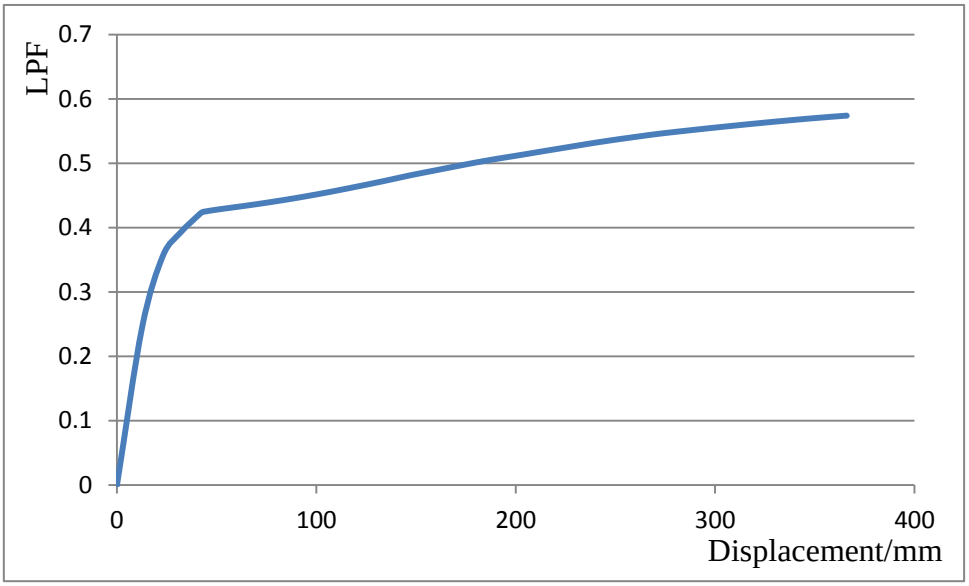

Figure 4.17 the LPF and global displacement relation

From the Figure 4.17 it is seen that in the curve at the first stage displacement changes little while the LPF rises sharply, and then the slope of the curves become smaller. This is similar with the result of the specialization project. But in fact they are different, for which non-linear effect has been taken into account, and the result can be explained by the figures below.

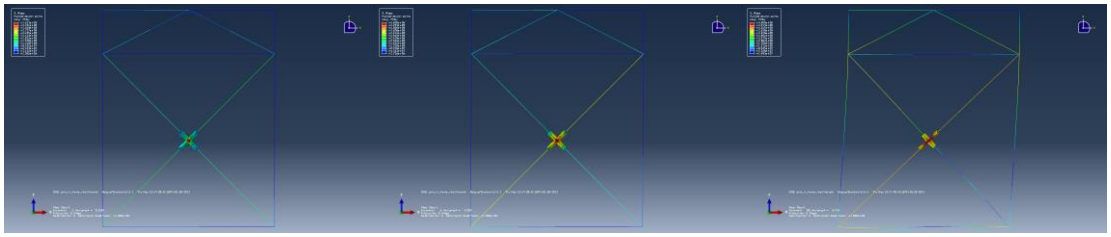

Figure 4.18 deformation and plots of stresses of the frame in different stages

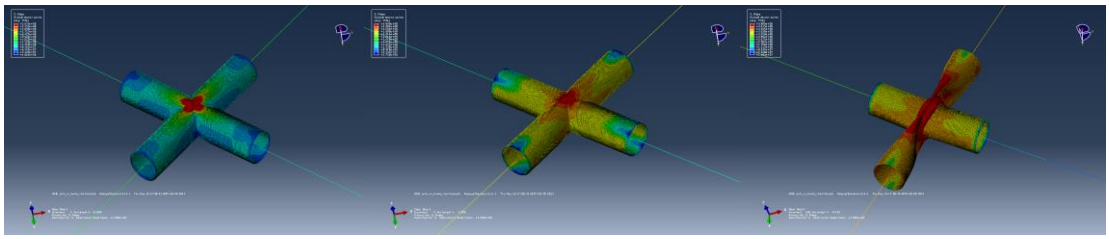

Figure 4.19 deformation and plots of stresses of the joint in frame in different stages

From the Figure 4.18, it is not difficult to see that the joint fails before the total frame system fails, i.e. the frame doesn't show buckle yet. The two compression braces squeeze the tension brace very seriously. At the very end of the simulation they even touch each other, and compress the tension brace to the opposite direction, which doesn't meet the actual condition. This indicates that the joint without a through member is weak and its capacity is not so satisfactory.

5) The new single joint as a part of a frame system

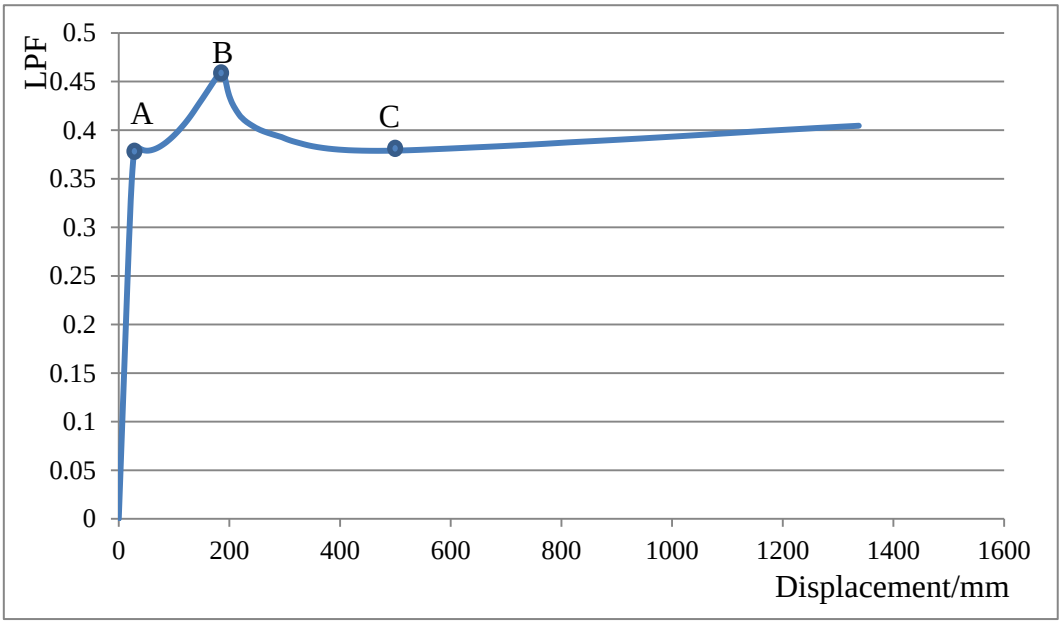

Figure 4.20 LPF-displacement relation

The curve in Figure 4.20 has 3 extreme points, dividing the whole process into 4 stages. Pictures in Figure 4.22 show the detail of the joint in different stages in correspondence with Figure 4.21.

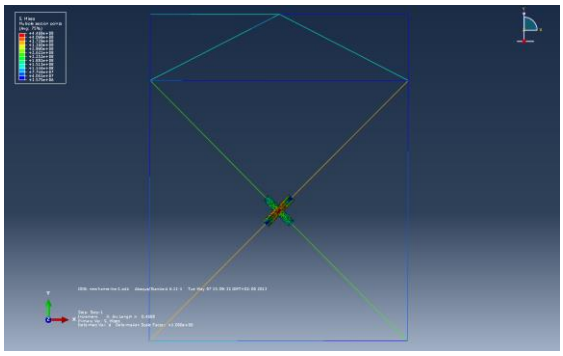

a.1st stage

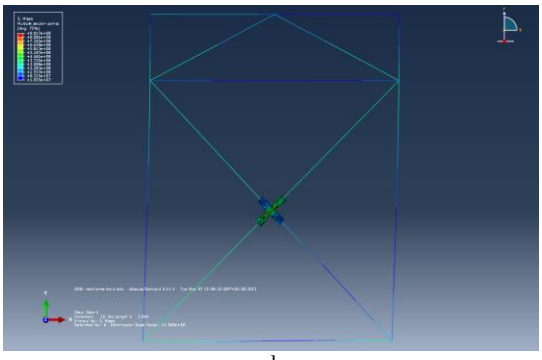

b.2nd stage

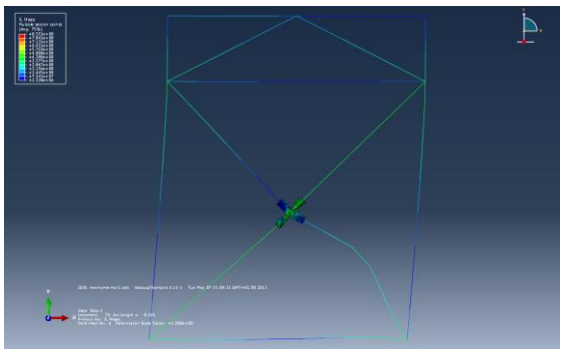

c. 3rd stage

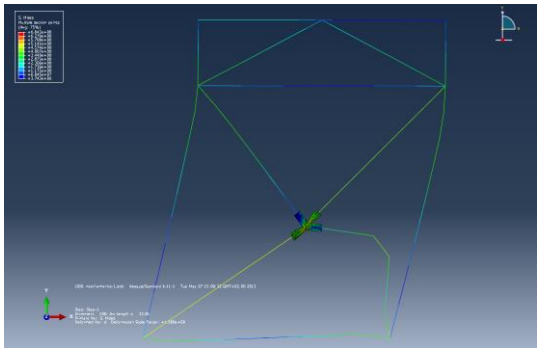

d. 4th stage

Figure 4.21 deformation and plots of stresses of the frame in different stages

In Figure 4.21(a), the whole frame starts to deform, and yielding occurs in the joint, which corresponds to point A in Figure 4.20.

In Figure 4.21(b), the frame has tilted to a certain extent, and the lower brace in compression starts to buckle and can take no more load corresponding to point B in Figure 4.20.

In figure 4.21(c), the frame system starts to regain strength because the rest of braces take the load instead, which corresponds to point C.

Figure 4.21(d) shows the end of the simulation, and the frame system has undergone a drastic shift compared to the initial position.

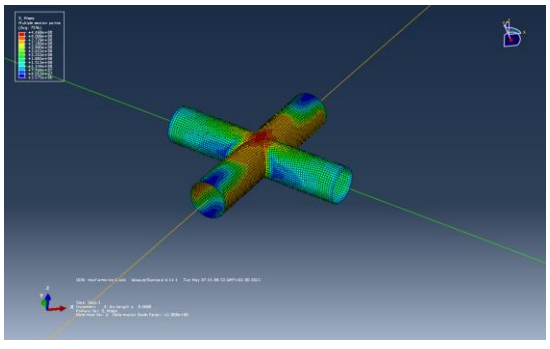

a. 1st stage

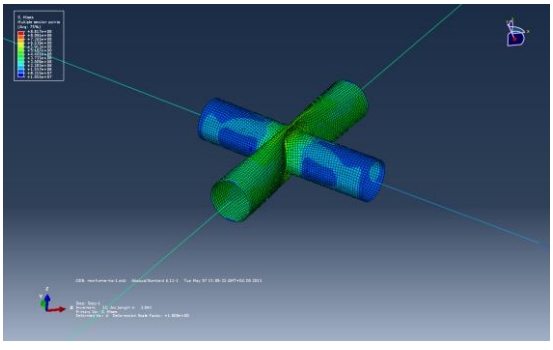

b. 2nd stage

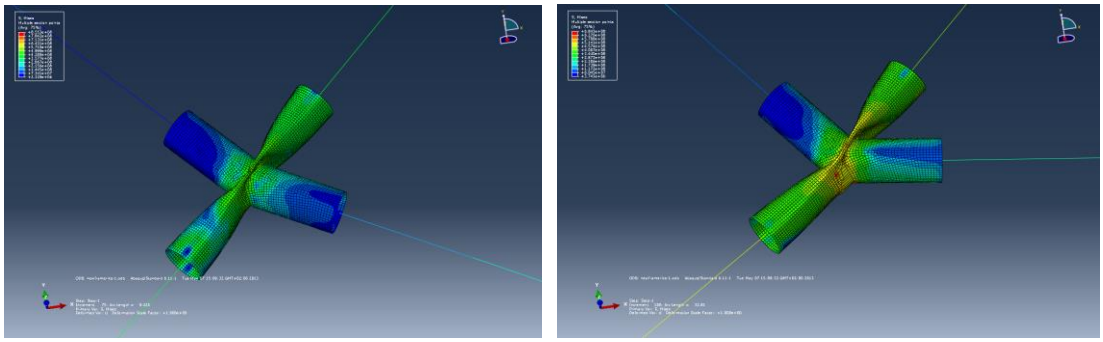

c. 3rd stage d. 4th stage

Figure 4.22 the detail of the joint in frame in different stages in correspondence with Figure 4.20

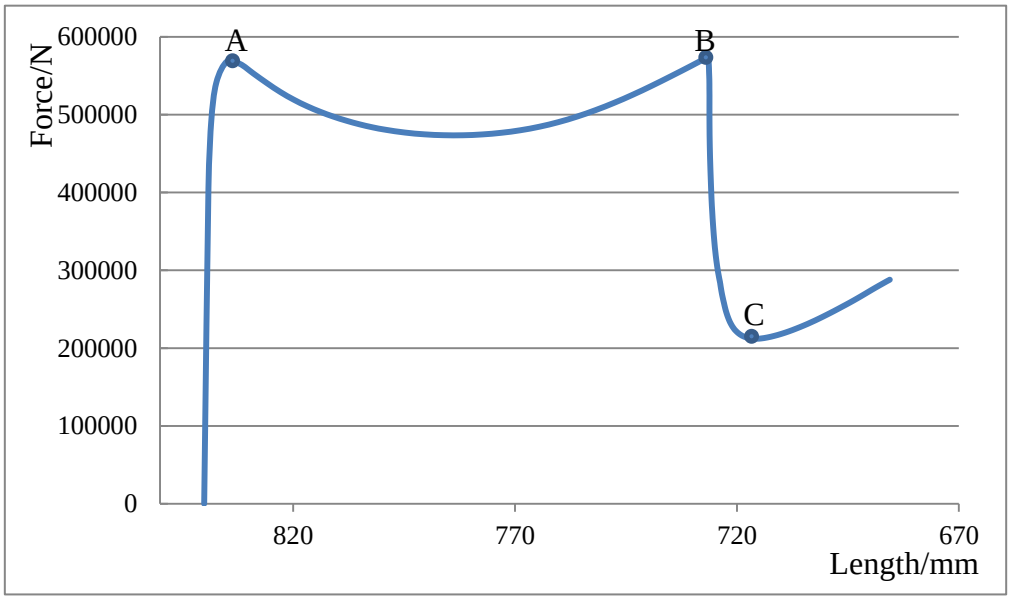

Figure 4.23 the relationship of the axial force of the upper compression brace and the length of the compression joint brace

Figure 4.23 shows the relationship of the axial force of the upper compression brace and the length of the compression joint brace (rotate deformation of the joint neglected). Similar with the force-displacement curve of new single joint as a part of a frame system, it has also 3 extreme points (Yielding occurs at Point A, Buckle starts at Point B, and the brace starts regaining strength at Point C).

6) Strain development of the joint

In order to study the strain of the joint, 3 sets are created to observe the strain development of different position of the joint, the positions of which are shown in Fig. 4.24.

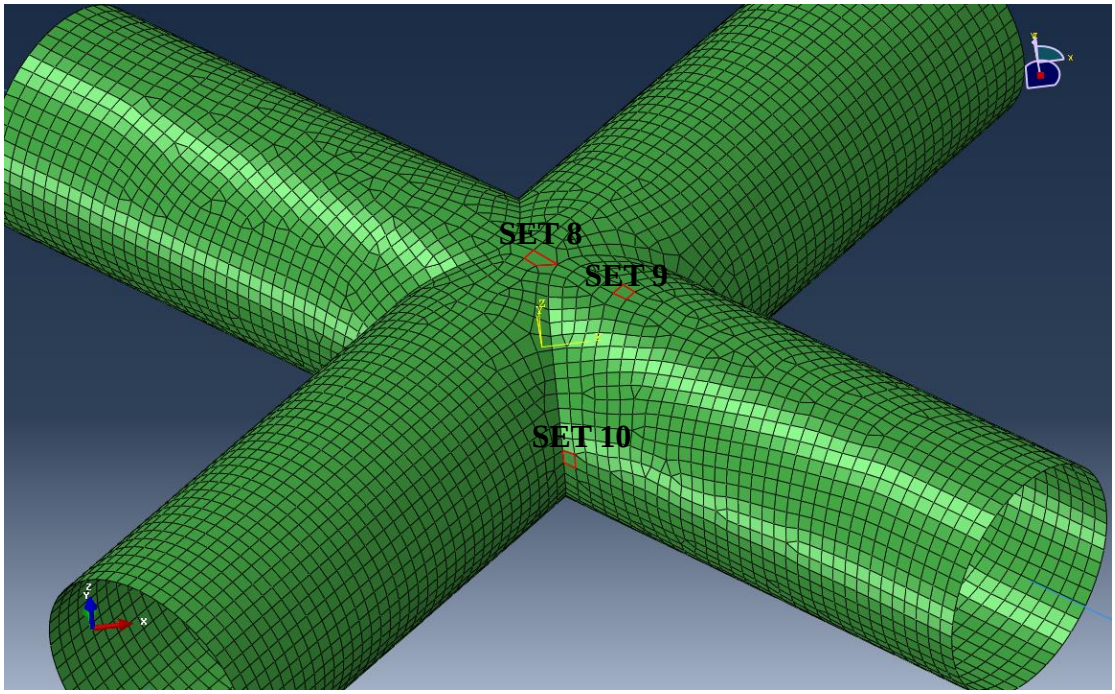

Figure 4.24 positions of the sets created in ABAQUS

According to Hagbart S. Alsos[36], The BWH criterion is made dependent on the mesh size, in order to imitate fracture after onset of local necking. The equivalent strain at fracture is illustrated in terms of the element size in Figure 4.25.

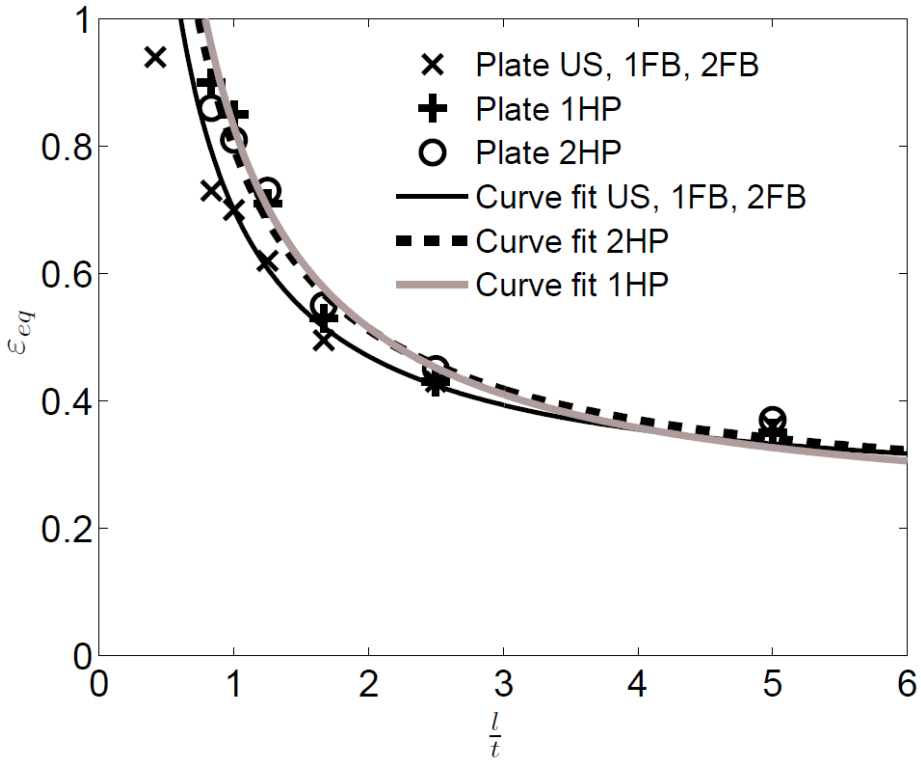

Figure 4.25 Equivalent plastic failure strains for different element sizes

In this case $\frac{l}{t}$=0.67, therefore as a estimation, the joint starts to fail when strain of some place reaches 0.8 approximately.

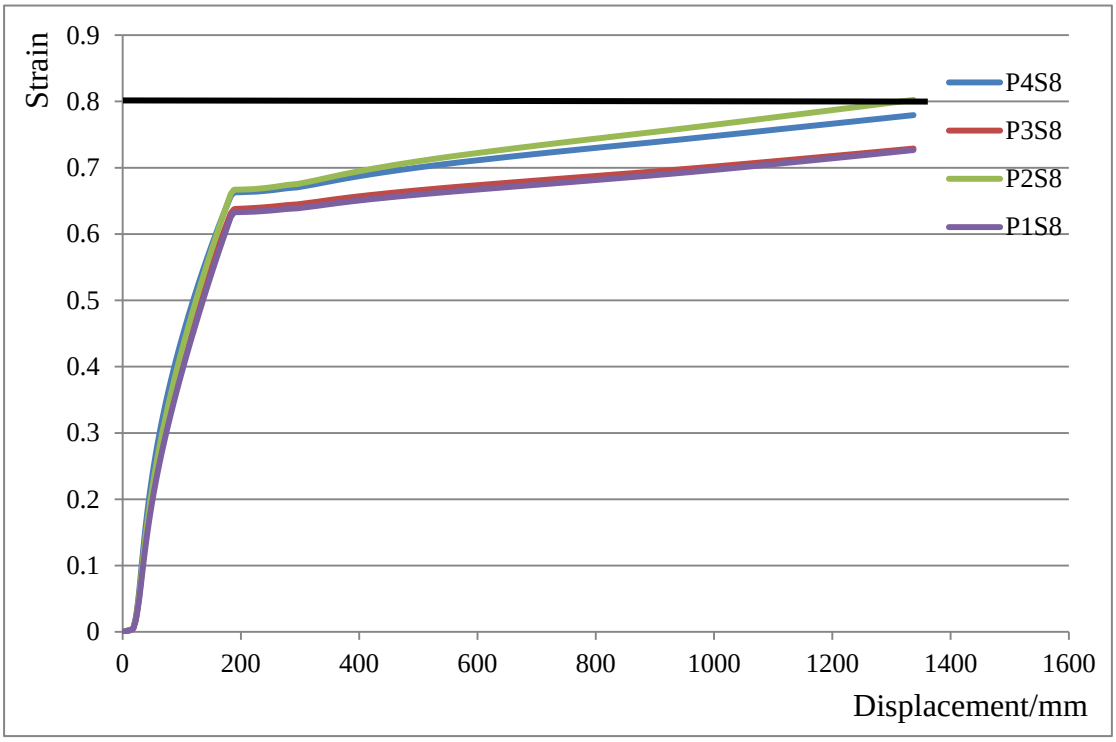

Figure 4.26 Strain-displacement relations of 4 nodes of set 8

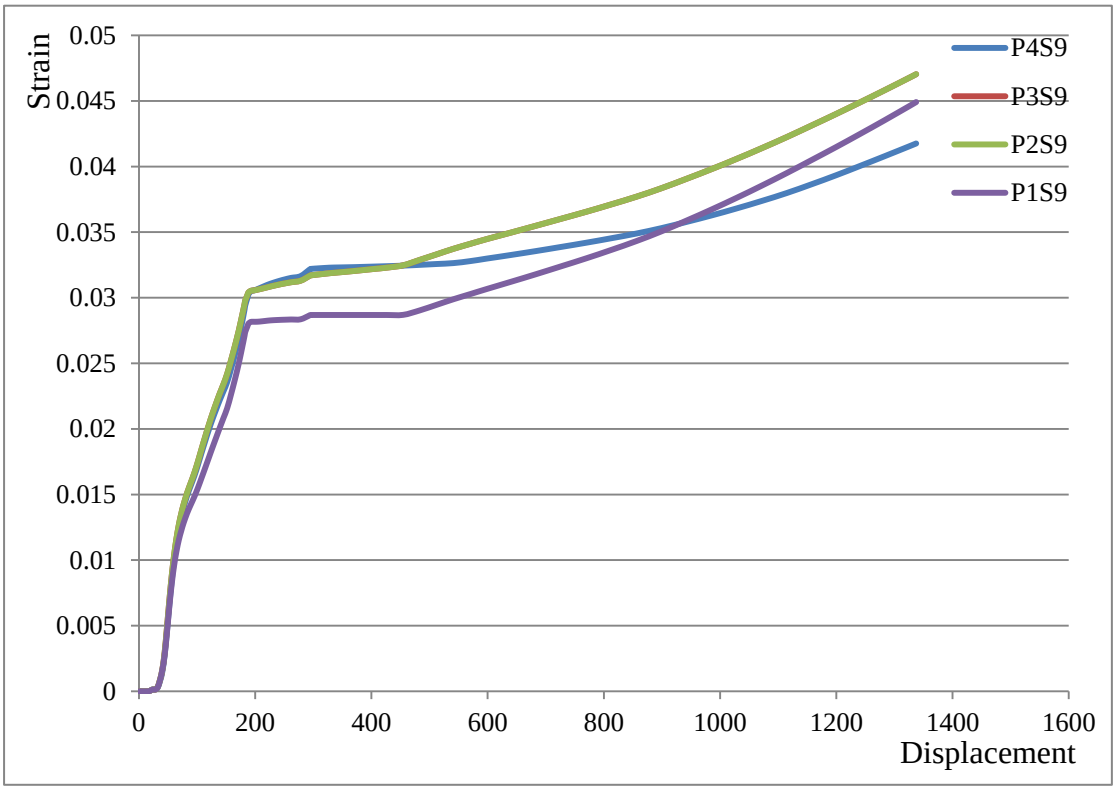

Figure 4.27 Strain-displacement relations of 4 nodes of set 9

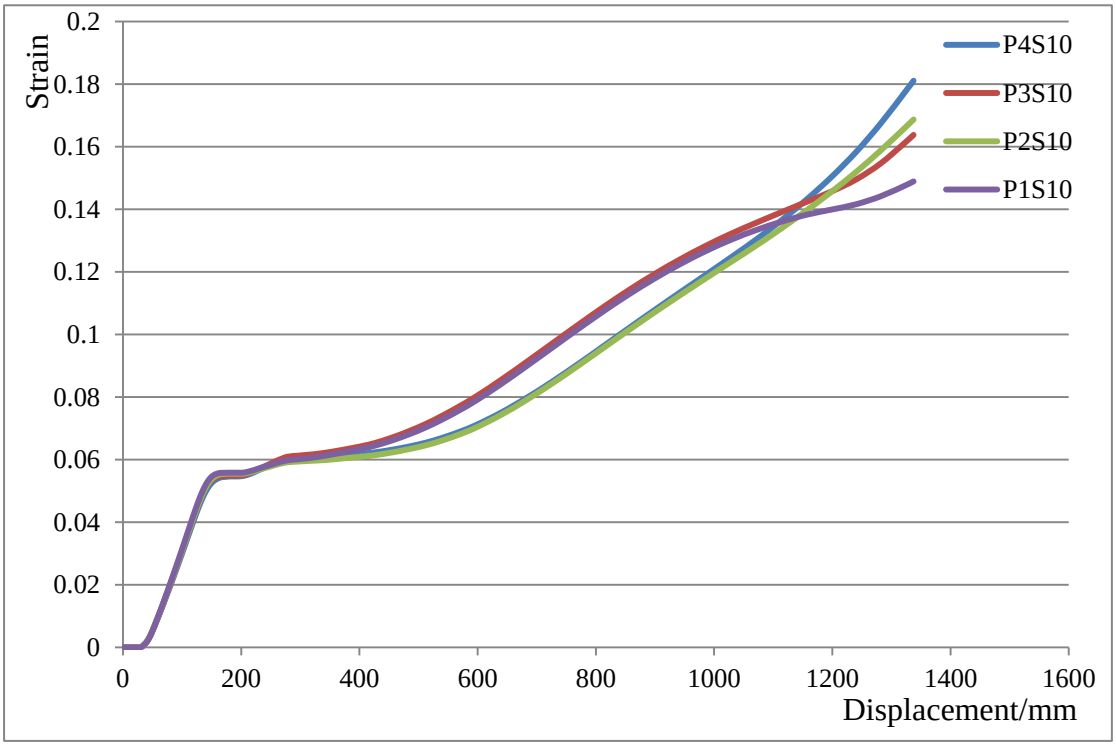

Figure 4.28 Strain-displacement relations of 4 nodes of set 10

Figure 4.26 to 4.28 show the relationship of strain and global displacement. Set 8 shows the largest strain, which can be explained by that it has the largest deformation due to the extrusion of the braces. And also it reaches the critical strain limit (0.8). This means that the ductility of set 8's position is the most critical and starts to fail, and should be strengthened to meet the strength requirements.

A comparative analysis

As a comparison, the joint model is rotated by 90 degree to let the through member in compression.

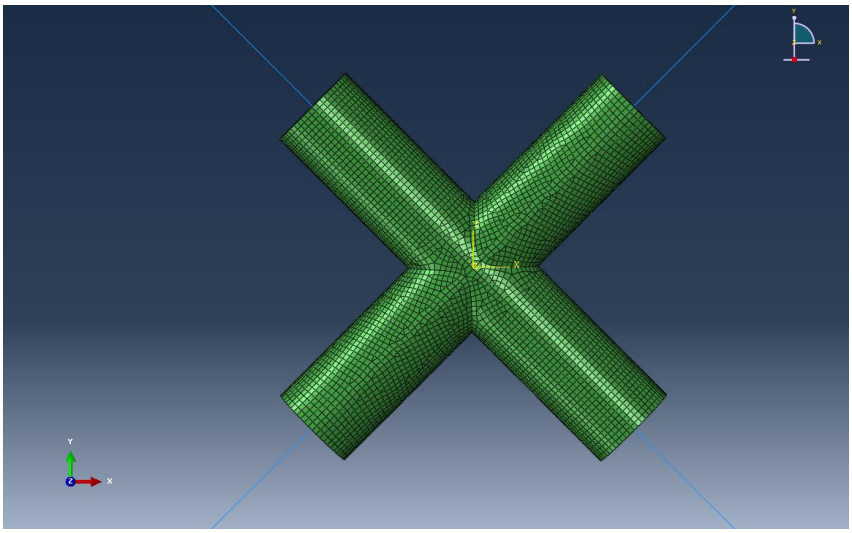

Figure 4.29 Rotated joint

The force-displacement curve are shown in Figure 4.30.

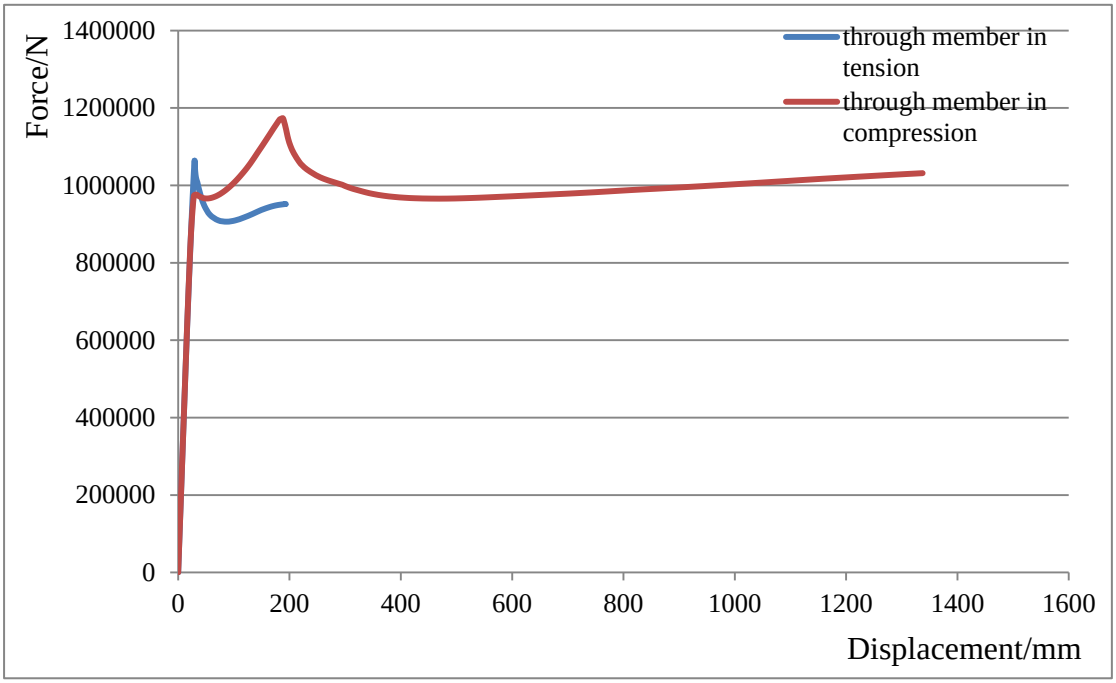

Figure 4.30 Comparison of the force-displacement curves

From the figure it is easy to see that if through member is made in compression, the critical load when yielding occurs is larger than when it is made in tension. And the displacement of the frame is much smaller than the previous one. This is because the buckling of the braces is out-of-plane buckling, while the previous one is in-plane buckling. That means that this kind of frame is more stable than previous one.

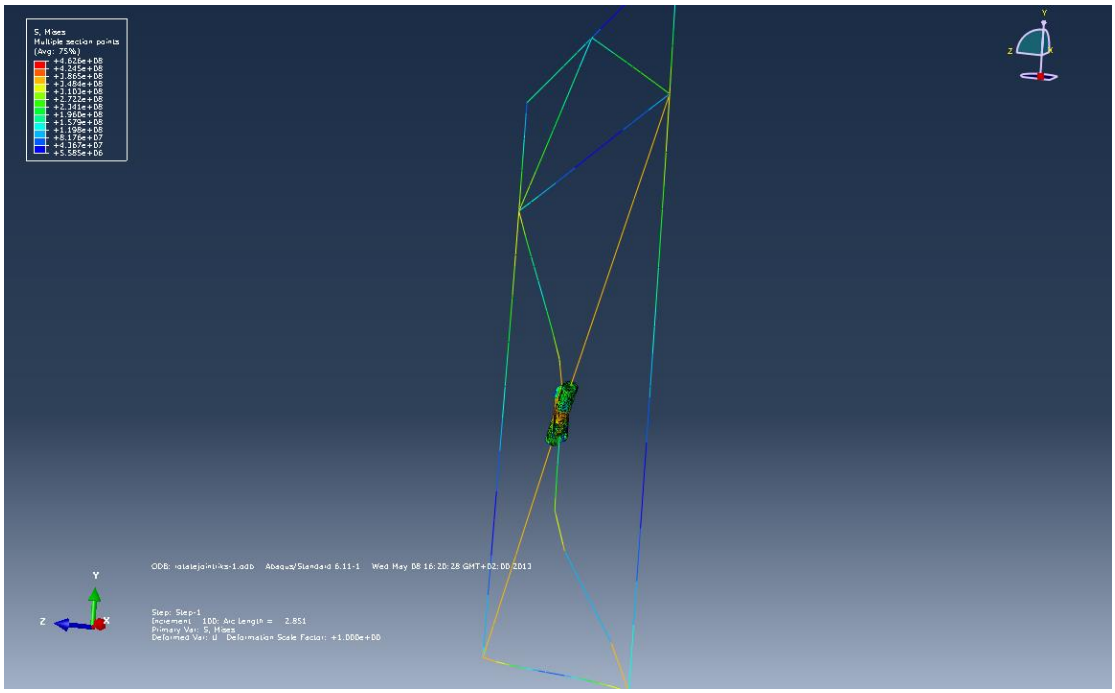

Figure 4.31 out-of-plane buckling

5. Conclusions

The two main objectives of this thesis have been to review of MSL joint strength formulations and to perform simulation with ABAQUS of various joints verify the simulation procedure with respect to force-deformation behavior and strain development and to contribute to the development of the data basis.

From the review of the MSL joint strength formulations revealed the current regulations of the joints about the resistance, ductility, etc. The ductility limit is reached before ultimate strength, which is conservative after the simulation by ABAQUS.

Simulation with ABAQUS shows some interesting results. The X-joints show very good ductility feature which is far beyond the ductility limits recommended by codes and regulations. That means after the joints' deformation exceed the ductility limits, they still have fairly sufficient capacity to resist deformation.

The force-displacement curves are more reasonable after non-linear effects are taken into account.

A joint without a through member shows a weaker capacity than the one with a through member, which means that a through-member joint can make better contribution to the strength of the structure than a non-through-member joint does when in same condition.

The behavior of the joint is different when analyzed independently from when in frame system. The reason is that when a single joint is analyzed, the force doesn't change direction. While in a frame system, the braces has a significant influence to the joint, as the braces can buckle, rotate, etc. which changes the direction of the force acting on the joints.

When the through member is in tension, the other two braces will compress it to a very large extent, which leads to a large strain development. That can also explain why the frame system is more stable when the joint is rotated by 90 degree. It is the most critical condition when the separate braces are in compression, which should be avoided in reality.

6. Recommendations for further work

Far from enough verification and validation is done. Also more variables need to be controlled and analyzed.

In this paper, only X-joints are analyzed, and the X-joints are the simplest ones, i.e. the two braces are of same length, diameter and wall thickness. In the future, other types of joints such as T joints or K joints may also be analyzed and compared. Also different brace geometry can be applied to see the effect they have to the joints capacity.

Due to limited time, analysis of the frame with usfos nonlinear joint has not been finished. So it is necessary to do it in the future.

In addition, the conservativeness concluded in this paper shows that current codes and regulations may be recommended to modify to reduce the conservativeness.

Reference

[1] NORSOK STANDARD, N-004 Rev. 2, October 2004, Design of steel structures.
[2] OMAE2011, Proceedings of the ASME201130th International Conference on Ocean, Offshore and Arctic Engineering, June 19-24, 2011, OMAE2011-49874, Safety Format and Acceptance Criteria for Analysis of Marine Structures Using Non-linear Methods.
[3]-[7] Jørgen Amdahl, FRAME STUDY, Chapter 8.
[8] Van der Vegte, G.J. (1995). The static strength of uniplanar and multiplanar tubular T- and X-joints, PhD thesis, Delft University of Technology, The Netherlands.
[9] USFOS Manual, USFOS Joint Capacity Theory, Description of use Verification.
[10]Hagbart S.Alsos (2007) Analytical and numerical analysis of sheet metal instability using a stress based criterion
[11] Keeler, S.P., Backhofen,W.A., 1964. Plastic instability and fracture in sheet stretched over rigid punches. ASM Transactions Quarterly 56,
25–48.
[12] Goodwin, G.M., 1968. Application of strain analysis to sheet metal forming in the press shop. In: SAE paper 680093.
[13][15][24]Ghosh, A.K., Laukonis, J.V., 1976. The influence of strain path changes on the formability of sheet steel. In: 9th Biennial Congress of the IDDRG, Sheet Metal Forming and Energy Conservation. ASM Publication.
[14][17][25] Graf, A.F., Hosford, W.F., 1993. Calculations of forming limit diagrams for changing strain paths. Metal Transactions A 24, 2497–2501.
[16] Barata da Rocha, A., Barlat, F., Jalinier, J.M., 1985. Prediction of the forming limit diagram of anisotropic sheets in linear and non-linear loading. Materials Science and Engineering 68, 151–164.
[18] Arrieux, R., Bedrin, C., Boivin, M., 1982. Determination of an intrinsic forming limit stress diagram for isotropic metal sheets. In:Proceedings of the 12th Biennial Congress IDDRG, pp. 61–71.
[19][26] Stoughton, T.B., 2001. Stress-based forming limits in sheet metal forming. Journal of Engineering Materials and Science 123, 417–422.
[20][27][29]Stoughton, T.B., Zhu, X., 2004. Review of theoretical models of the strain-based fld and their relevance to the stress-based fld. International Journal of Plasticity 20, 1463–1486.
[21] Wu, P.D., Graf, MacEwen, S.R., Lloyd, D.J., Jain, M., Neale, K.W., 2005. On forming limit stress diagram analysis. International Journal of Solids and Structures 42, 2225–2241.
[22] Hallquist, J., 2007a. Ls-dyna keyword users manual—ls971. Technical report, Livemore Software.
Hallquist, J., 2007b. Ls-dyna theory manual— ls971. Technical report, Livemore Software.

[23] Tornqvist, R., 2003. Design of crashworthy ship structures. Ph.D. thesis, DTU.
[28] Hill, R., 1952. On discontinuous plastic states with special reference to localized necking in thin sheets. Journal of the Mechanics and Physics of Solids 1, 19–30.
[30] Marciniak, Z., Kuczynski, K., 1967. Limit strains in processes of stretch forming sheet metal. Journal of Mechanical Sciences 9, 609–620.
[31] [32] Bressan, J.D., Williams, J.A., 1983. The use of a shear instability criterion to predict local necking in sheet metal deformation. International Journal of Mechanical Science 25, 155–168.
[33] Brunet, M., Clerc, P., 2007. Two prediction methods for ductile sheet metal failure. In: ESAFORM Conference on Material Forming.
[34] TMR4305 Chapter 12 - Nonlinear Analysis
[35] ABAQUS Users' Manual
[36] Hagbart S. Alsos , Ship Grounding,Analysis of Ductile Fracture, Bottom Damage and Hull Girder Response, PHD Thesis, NTNU On the resistance to penetration of stiffened plates, Part II – Numerical analysis